Time dependent source apportionment of submicron organic aerosol for a rural site in an alpine valley using a rolling PMF window

Gang Chen[1], Yulia Sosedova[1,2], Francesco Canonaco[1,2], Roman Fröhlich[1], Anna Tobler[1,2], Athanasia Vlachou[1], Kaspar R. Daellenbach[1], Carlo Bozzetti[2], Christoph Hueglin[3], Peter Graf[3], Urs Baltensperger[1], Jay G. Slowik[1], Imad El Haddad[1], and André S.H. Prévôt[1*]

[1]Laboratory of Atmospheric Chemistry, Paul Scherrer Institute, CH-5232 Villigen PSI, Switzerland

[2]Datalystica Ltd., Park innovAARE, CH-5234 Villigen, Switzerland

[3]Empa, Swiss Federal Laboratories for Materials Science and Technology, Laboratory for Air Pollution and Environmental Technology, CH-8600 Dübendorf, Switzerland

**Correspondence to:* André S. H. Prévôt (andre.prevot@psi.ch)

Abstract

We collected one year of aerosol chemical speciation monitor (ACSM) data in Magadino, a village located in the south of the Swiss Alpine region, one of Switzerland's most polluted areas. We analysed the mass spectra of organic aerosol (OA) by positive matrix factorisation (PMF) using source finder professional (SoFi Pro) to retrieve the origins of OA. Therein, we deployed the rolling algorithm to account for the temporal changes of the source profiles, which is closer to the measurement. As the first-ever application of rolling PMF with ME-2 analysis on a yearlong dataset that was collected from a rural site, we resolved two primary OA factors (traffic-related hydrocarbon-like OA (HOA) and biomass burning OA (BBOA)), one mass-to-charge ratio (*m/z*) 58 related OA (58-OA) factor, a less oxidised oxygenated OA (LO-OOA) factor, and a more oxidised oxygenated OA (MO-OOA) factor. HOA showed stable contributions to the total OA through the whole year ranging from 8.1 to 10.1%, while the contribution of BBOA showed a clear seasonal variation with a range of 8.3–27.4% (highest during winter, lowest during summer) and a yearly average of 17.1%. OOA (sum of LO-OOA and MO-OOA) contributed 71.6% of the OA mass, varying from 62.5% (in winter) to 78% (in spring and summer). The uncertainties (σ) for the modelled OA factors (i.e., rotational uncertainty and statistical variability of the sources) varied from ±4% (58-OA) to a maximum of ± 40% (LO-OOA). Considering that BBOA and LO-OOA (showing influences of biomass burning in winter) had significant contributions to the total OA mass, we suggest reducing and controlling the residential heating as a mitigation strategy for better air quality and lower PM levels in this region and similar locations. In Appendix A, we conducted a head-to-head comparison between the conventional seasonal PMF analysis and the rolling mechanism. We found similar or slightly improved results in terms of mass concentrations, correlations with external tracers and factor profiles of the constrained POA factors. The rolling results show smaller scaled residuals and enhanced correlations between OOA factors and corresponding

inorganic salts than those of the seasonal solutions, which was most likely because the rolling PMF analysis can capture the temporal variations of the oxidation processes for OOA components. Specifically, the time dependent factor profiles of MO-OOA and LO-OOA can well explain the temporal viabilities of two main ions for OOA factors, *m/z* 44 (CO_2^+) and *m/z* 43 (mostly $C_2H_3O^+$). This rolling PMF analysis, therefore, provides a more realistic source apportionment (SA) solution with time dependent OA sources. The rolling results also show good agreement with offline Aerodyne aerosol mass spectrometer (AMS) SA results from filter samples, except for winter. The latter discrepancy is likely because the online measurement is capable of capturing the fast oxidation processes of biomass burning sources, in contrast to the 24-hour filter samples. This study demonstrates the strengths of the rolling mechanism and provides a comprehensive criterion list for ACSM users to obtain reproducible SA results, and is a role model for similar analyses of such worldwide available data.

1 Introduction

Atmospheric particulate matter (PM) affects human health and climate. In particular, it influences the radiative balance (IPCC, 2014; von Schneidemesser et al., 2015), reduces visibility (Chow et al., 2002; Horvath, 1993), and negatively affects human health by triggering respiratory and cardiovascular diseases and allergies (Daellenbach et al., 2020; Dockery and Pope, 1994; Mauderly and Chow, 2008; Monn, 2001; Pope and Dockery, 2006; von Schneidemesser et al., 2015). Fine PM exposure strongly correlates with the global mortality rate. Lelieveld et al. (2015) estimated that outdoor air pollution, mostly $PM_{2.5}$ (PM with an aerodynamic diameter smaller than 2.5 μm), causes 3.3 million premature deaths per year worldwide. Despite this correlation, different aerosol sources may have strongly different effects on health (Daellenbach et al., 2020). Thus, both climate and health effects are affected by particle chemical composition, which is related to emission sources of primary particles and

63 precursor gases for secondary aerosol (IPCC, 2014; Jacobson et al., 2000; Jacobson, 2001;
64 Lelieveld et al., 2015; Ramanathan et al., 2005).

65 Organic aerosol (OA) constitutes 20–90% of fine PM (Jimenez et al., 2009; Murphy et al.,
66 2006; Zhang et al., 2007) and contains millions of chemical compounds. Since OA is subject
67 of an extremely complex mixture of chemical constituents, with highly dynamic spatial and
68 temporal (seasonal, diurnal, etc.) variability of directly emitted particles and gas-phase
69 precursors and a complex chemical processing in the atmosphere, elucidation of the chemical
70 composition and physical properties of OA remains challenging. Identification and
71 quantification of OA sources with a sophisticated interpolation of spatial and temporal
72 variabilities are essential for developing effective mitigation strategies for air pollution and a
73 better assessment of the aerosol effect on both health and climate.

74 OA source apportionment (SA) and PM composition have been studied extensively using the
75 Aerodyne aerosol mass spectrometer (AMS) (Canagaratna et al., 2007). However, due to the
76 complexity of the AMS measurements and their high operational expenses, AMS campaigns
77 are often limited to short periods of a few weeks to months. The aerosol chemical speciation
78 monitor (ACSM) allows for unattended long-term observation (>1 year) of non-refractory
79 aerosol particles (Ng et al., 2011a; Fröhlich et al., 2013). It also makes it possible to investigate
80 the long-term temporal variations of OA sources, which is crucial for policymakers to introduce
81 or validate aerosol-related environmental policies.

82 Positive matrix factorisation (PMF, see Section 3.1 in the Supplement) has been used in various
83 studies for SA of OA (Lanz et al., 2007; Aiken et al., 2009; Hildebrandt et al., 2011; Zhang et
84 al., 2011;Mohr et al., 2012; Schurman et al., 2015). The multilinear engine (ME-2)
85 implementation of PMF (Paatero, 1999) improves model performance by allowing the use of
86 *a priori* information (constraints on source profiles and/or time series) to direct the model

towards environmentally meaningful solutions (Canonaco et al., 2013; Crippa et al., 2014; Fröhlich et al., 2015; Lanz et al., 2008; Ripoll et al., 2015). For long-term data (one year or more) with high time resolution, the composition of a given source could change considerably due to the meteorological and seasonal variabilities. However, a major limitation of PMF is the assumption of static factor profiles, such that it fails to respond to these temporal changes. Therefore, long-term chemically speciated data have been evaluated monthly or seasonally (Petit et al., 2014; Canonaco et al., 2015; Minguillón et al., 2015; Ripoll et al., 2015; Bressi et al., 2016; Reyes-Villegas et al., 2016) to at least take the seasonal variations into account. To improve the analysis of long-term ACSM datasets, a novel approach that utilises PMF analysis on a shorter time rolling window was first proposed by Parworth et al. (2015) and further refined using ME-2 by Canonaco et al. (2021). The short length of the rolling PMF window allows the PMF model to take the temporal variations of the source profiles into account (e.g., biogenic versus domestic burning influences on oxygenated organic aerosol (OOA)), which normally provides better separation between OA factors. In addition, using this technique together with bootstrap resampling and a random *a*-value approach allows users to assess the statistical and rotational uncertainties of the PMF results (Canonaco et al., 2021; Tobler et al., 2020).

In this work, we conducted a one-year ACSM measurement from September 2013 to October 2014 in Magadino, located in an alpine valley in southern Switzerland. We present a comprehensive analysis of the ACSM dataset measured in Magadino using a novel PMF technique, the “rolling PMF”. In addition, we also compare the results of the rolling PMF with the source apportionment of offline AMS filter samples (Vlachou et al., 2018) and conventional seasonal PMF analysis.

2 Methodology

2.1 Sampling site

Magadino is in a Swiss alpine valley (46°90'37'' N, 85°60'2'' E, 204 m.a.s.l.), where the sampling site located. This site belongs to the Swiss National Air Pollution Monitoring Network (NABEL, https://www.empa.ch/web/s503/nabel). It is around 1.4 km away from the local train station, Cadenazzo, around 7 km away from the Locarno Airport, and nearly 8 km away from the Lake Maggiore. This station is surrounded by agricultural fields within a rural area, and is considered as a rural background site. It can be potentially affected by domestic wood burning, adjacent agricultural activity and transit traffic through the valley. The site topography favours quite high PM levels due to stagnant meteorological conditions or boundary layer inversions, especially in winter. The annual average PM_{10} concentration in Magadino exceeded the annual average PM_{10} limit value for Switzerland (20 $\mu g \cdot m^{-3}$) for five years out of the period 2007–2016 (Meteotest, 2017; The Swiss Federal Council, 2018).

2.2 ACSM measurements

In this study, chemical composition and mass loadings of non-refractory constituents of ambient submicron aerosol particles (NR-PM_1) were measured by an Aerodyne quadrupole ACSM (Ng et al., 2011a). The ACSM uses the same sampling and detection technology as the AMS but is simplified and designated for long-term monitoring applications by reducing maintenance frequency at the cost of lower sensitivity, restriction to integer mass resolution, and no size measurement. Same as for the AMS, sampled submicron particles enter the instrument through a critical orifice (100 µm I.D.) at a flow rate of 1.4 $cm^3\ s^{-1}$ (at 20 °C and 1 atm). The sampling flow will pass either through a particle filter or directly into the system using an automated 3-way switching valve that is switched every ~30 s. An aerodynamic lens focuses the sampled particles into a narrow beam which impact on a tungsten surface of around 600 °C, where the non-refractory particles vaporise and are subsequently ionised by an electron

impact source (70 eV). The resulting ions are detected by a quadrupole mass-spectrometer up to a mass-to-charge ratio (*m/z*) of 148 Th. The particle mass spectrum is represented by the difference between the total ambient air signal and the particle-free signal.

The quantification of ACSM data requires an estimation of the fraction of NR-PM_1 that bounces off the oven without being vaporised and therefore is not detected (Canagaratna et al., 2007; Matthew et al., 2008). In this study, a constant collection efficiency (CE) factor of 0.45 was applied to take it into account. The details of determinations of CE value was described in Section 1 in the Supplement. In this study, we recorded the data with a time resolution of 30 minutes. During the campaign, the ACSM filament burnt out on 14 April 2014. This was addressed by switching to the backup filament installed within the instrument (no venting required). Calibration of the relative ionisation efficiencies (RIE) of particulate nitrate, sulphate, and ammonium were conducted using size-selected (300 nm) pure NH_4NO_3 and pure $(NH_4)_2SO_4$ particles. Calibrations of the RIE, *m/z* scale, and the sampling flow were performed every 2 months. In this study, we used the averaged RIEs for nitrate, sulphate, and ammonium, the exact values are shown in **Fig S1** of the Supplement.

2.3 Complementary measurements

Meteorological data, including temperature, precipitation, wind speed, wind direction, and solar radiation are monitored at the NABEL station. In addition, concentrations of trace gases (SO_2, O_3, NO_x), equivalent black carbon (eBC), and PM_{10} were measured with a time resolution of 10 minutes. We used an aethalometer (AE 31 model by Magee Scientific Inc.) to measure eBC concentrations. Therefore, we conducted SA of eBC by following Zotter et al. (2017) using Ångstrom exponents for eBC from traffic $\alpha_{tr} = 0.9$ and wood burning $\alpha_{wb} = 1.68$. More details about eBC source apportionment are provided in Section 2 of the Supplement.

2.4 Preparation of the data and error matrices for PMF

In this study, we used acsm_local_1610 software (Aerodyne Research Inc.) to prepare the PMF input matrix. In total, this dataset includes 19'708 time points and 67 ions. Of these, CO_2^+-related variables (I_{O+} (m/z = 16), I_{HO+} (m/z = 17), and I_{H2O+} (m/z = 18)) were excluded from the spectral matrix prior to a PMF analysis. They are reinserted into the OA factor mass spectra after the PMF analysis using the ratio from the fragmentation table (Allan et al., 2004); the factor concentrations are likewise adjusted. According to Allan et al. (2003, 2004), the measurement error matrix was calculated with a minimum error considered for the uncertainty of all variables in the data matrix as in Ulbrich et al. (2009). Following the recommendations in Paatero and Hopke (2003) and Ulbrich et al. (2009), the measurement uncertainty for variables (m/z) with a signal-to-noise ratio (S/N) < 2 (weak variables) and S/N < 0.2 (bad variables) were increased by a factor of 2 and 10, respectively. In total, 27 weak ACSM variables were down-weighted. Additionally, m/z 12 and 13 were not considered during the PMF analyses due to being noisy and their overall negative signal. Moreover, m/z 15 was not only very noisy (S/N = 0.09) but maybe also affected by high biases due to potential interference with air signals.

2.5 Rolling PMF analysis with ME-2

In this study, we conducted a series of steps (Section 3.2 and 3.3 in the Supplement) to obtain the results we presented in this manuscript. In summary, we first tested potential sources for each season with seasonal PMF *pre-tests*, secondly, we obtained stable seasonal solutions from bootstrap seasonal analysis. Then, we conducted rolling PMF with certain settings (constraints, number of repeats, length of the window size, and step of rolling window). Lastly, we were able to retrieve robust results using specific criteria to define environmental reasonable solutions. Please refer to Section 3.2 and 3.3 in the Supplement for more detailed description of each step. In this section, we focus on the general introduction of rolling PMF with ME-2,

183 the differences between our method vs. the method developed by Canonaco et al. (2021), and
184 the general settings of the rolling PMF analysis in this study.

185 Running PMF over the long-term ACSM datasets assumes that the OA source profiles are static
186 within this time window. It can lead to large errors since OA chemical fingerprints are expected
187 to vary over time (Paatero et al., 2014). For example, Canonaco et al. (2015) showed that the
188 variability of summer and winter OOA cannot be accurately represented by a single pair of
189 OOA profiles. A common way to reduce the model uncertainty arising from this source is to
190 choose a proper number of OA factors (Sug Park et al., 2000) and then perform a PMF analysis
191 on a subset of measurements to capture temporal features of OA chemical fingerprints. Such
192 characterisation of OA sources on a seasonal basis has been demonstrated in a number of
193 studies (Lanz et al., 2008; Crippa et al., 2014; Petit et al., 2014; Minguillón et al., 2015; Ripoll
194 et al., 2015; Zhang et al., 2019). Parworth et al. (2015) introduced the rolling PMF by running
195 PMF on a small window (14 days), which advanced with a step of 1 day. This novel technique
196 enables the source profiles to adapt to the temporal variabilities. Canonaco et al. (2021)
197 combined the rolling PMF technique with ME-2 (Section 3.1 in the Supplement) to deal with
198 the rotational ambiguity of the PMF analysis. In addition, it also used the bootstrap resampling
199 strategy (Efron, 1979) and random *a*-values (Section 3.2.2 in the Supplement) to estimate the
200 statistical and rotational uncertainties of the PMF analysis.

201 In this study, we mostly followed the methods developed by Canonaco et al. (2021), but with
202 some modifications. The settings of the rolling PMF window is explicitly explained in Section
203 3.2.3 of the Supplement). In addition, we also performed a test of rolling window size (i.e., 1,
204 7, 14, and 28 days) using a similar approach (Section 4 in the Supplement). As Canonaco et al.
205 (2021) did, we also used the criteria-based selection function developed by Canonaco et al.
206 (2021) to evaluate our PMF runs. The settings of the criteria are provided in Section 3.2.4 of
207 the Supplement.

However, instead of using published reference factor profiles like Canonaco et al. (2021) have done, we retrieved the reference profiles of primary and local factors from seasonal bootstrap analysis (Section 3.2 in the Supplement). Specifically, the reference profiles of hydrocarbon-like OA (HOA) factor and biomass burning OA (BBOA) factor were retrieved from winter (December, January, and February, DJF) bootstrapped PMF solution as shown in **Fig. S4**, and we got the *m/z* 58 related (58-OA) factor profile from summer (June, July, and August, JJA) bootstrapped PMF solution (**Fig. S4**). The 58-OA was dominated by nitrogen-containing fragments (at *m/z* 58, 84, and 98). In general, ACSM estimates organic *m/z* 98 signal by dividing organic *m/z* 84 to a factor of 2 according to the fragmentation table of organic species that was provided by Allan et al. (2004). Thus, the intensity of *m/z* 98 is always half of the intensity of *m/z* 84 in each factor. This 58-OA only appeared after the filament was switched on 14 April 2014. The instrument setup thus strongly influenced the sensitivity of these components due to influences of surface ionisation. The nitrogen-containing ion, *m/z* 58, was also observed in Hildebrandt et al. (2011) due to the enhanced surface ionisation in a certain period. In addition, the potassium signal enhanced at the same time, which further corroborated our hypothesis of the enhanced surface ionisation. Also, since this factor was constrained through the whole dataset, the PMF model overestimated the mass concentration of this factor significantly, which leads to high uncertainties for the 58-OA. Therefore, the time series of this source should be considered as the upper limit, and the real mass concentration of it could be substantially lower. However, with the low mass concentration of the 58-OA during the whole campaign, we considered it as a minor factor. Thus, this factor was considered in the PMF analysis, but no further interpretation of its potential source will be attempted in this manuscript Moreover, we took a different path to define “good” PMF solutions by using a novel student *t*-test approach to determine the environmentally reasonable solutions quantitatively with minimum subjective judgements (Section 3.3 in the Supplement). Overall, we provided a

comprehensive analysis of a long-term ACSM dataset using this state-of-the-art technique in this work. The results were unfolded in the following section.

3 Results and discussion

3.1 Overview of PM_1 sources in Magadino

Considering that the major part of eBC is within PM_1 (Schwarz et al., 2013), we added eBC to the total NR-PM_1 from the ACSM to perform a mass closure analysis using independent measurements of $PM_{2.5}$/PM_{10} from filters. The gravimetric $PM_{2.5}$ and PM_{10} show a high correlation with the total estimated PM_1 (NR-PM_1 +eBC) (**Fig. S1c**). The slopes of the linear fits (± 1 standard deviation) are 1.62 ± 0.05 (R^2 = 0.81, N=79) for $PM_{2.5}$ *vs.* PM_1 and 1.84 ± 0.03 (R^2 = 0.67, N=335) for PM_{10} *vs.* PM_1. It means that the estimated PM_1 comprised 62% and 54% of the $PM_{2.5}$ and PM_{10} mass, respectively. The daily averages of inorganic species concentrations measured by the ACSM and those measured on the filters by ion chromatography showed a good correlation, with R^2 = 0.83 for SO_4^{2-}, R^2 = 0.82 for NO_3^- and R^2 = 0.50 for Cl^-, with slopes close to 1 (**Fig. S1a**). The 2-week average of total ammonium and total nitrate measured by the offline AMS technique agreed rather well with the ACSM ammonium (R^2 = 0.47) and nitrate (R^2 = 0.79), as shown in the plots in **Fig. S1b**. The ion balance of particulate ammonium, sulphate and nitrate measured by the ACSM showed that the measured aerosol particles were mostly neutral.

The daily average PM_1 components are shown in **Fig. 1a**, with an annual average PM_1 concentration (including eBC) from September 2013 to October 2014 equal to 10.2 μg m^{-3}. In winter, the average PM_1 concentration was highest (13.8 μg·m^{-3}), with OA contributing 54% to the total PM_1 mass. In summer, the average PM_1 mass concentration was below 10 μg·m^{-3}, but the relative contribution of the OA fraction increased to 62%.

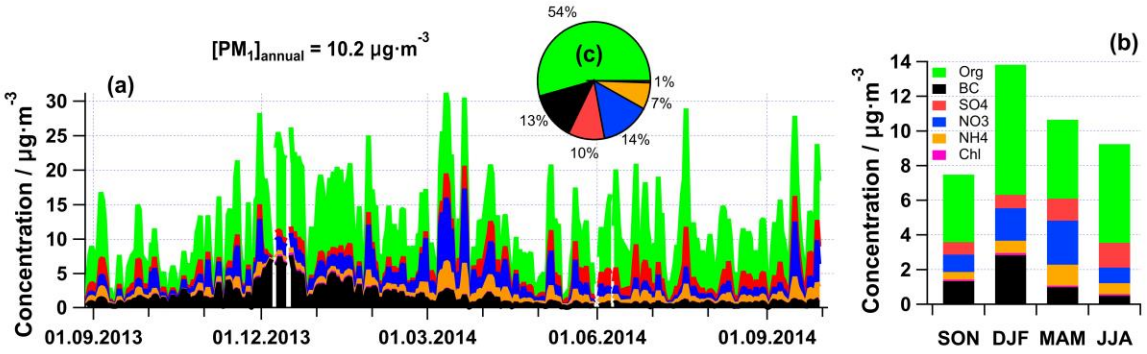

256

257 **Fig. 1** Chemical composition of PM_1 in Magadino 2013-2014 – daily (a), seasonal (b) and
258 annual (c) averages. The labels indicate non-refractory organics (Org), sulphate (SO_4), nitrate
259 (NO_3), ammonium (NH_4) and chloride (Cl) measured by the ACSM, and black carbon (BC)
260 measured by light absorption.

261

262 Seasonally averaged diurnal cycles of NR-PM_1 components and eBC are displayed in **Fig. 2**.
263 In this study, all the data is based on local time (Central European Time). In fall, spring and
264 summer, the diurnals of these pollutants seem to be mainly affected by the development of the
265 boundary layer height (BLH). Most of the species show similar diurnal trends for these three
266 seasons. In addition, summer has the highest sulphate concentration due to the enhanced
267 photochemical production. In winter, air pollutants are accumulated during the evening and
268 night due to the thermal inversion. In general, eBC and organics have higher levels due to
269 enhanced biomass burning emissions and a lower BLH. We observed distinct midday peaks of
270 organics, sulphate, nitrate, ammonium, chloride, and NO_x in the winter. Magadino experienced
271 a series of windless, cold, but sunny periods from December 2013 to January 2014, including
272 such sharp peaks (**Fig. S6a**). This was due to advection within the shallow boundary layer as
273 both primary and secondary pollutants increased simultaneously. At the same time, the local
274 wind speed near the ground was very low. One potential explanation was that the locally and
275 regionally induced orography influenced winds, including vertical diffusion processes, caused
276 these delayed midday peaks. However, these processes remain difficult to track without

277 spatially distributed measurements. Such phenomena were not observed during cloudy, cold,
278 and windless days (**Fig. S6b**) without thermally induced meteorological processes. Unlike
279 other seasons, the dilution process due to vertical mixing happened only after noon time due to
280 strong inversions during the night and late irradiation of the valley surface in the winter.

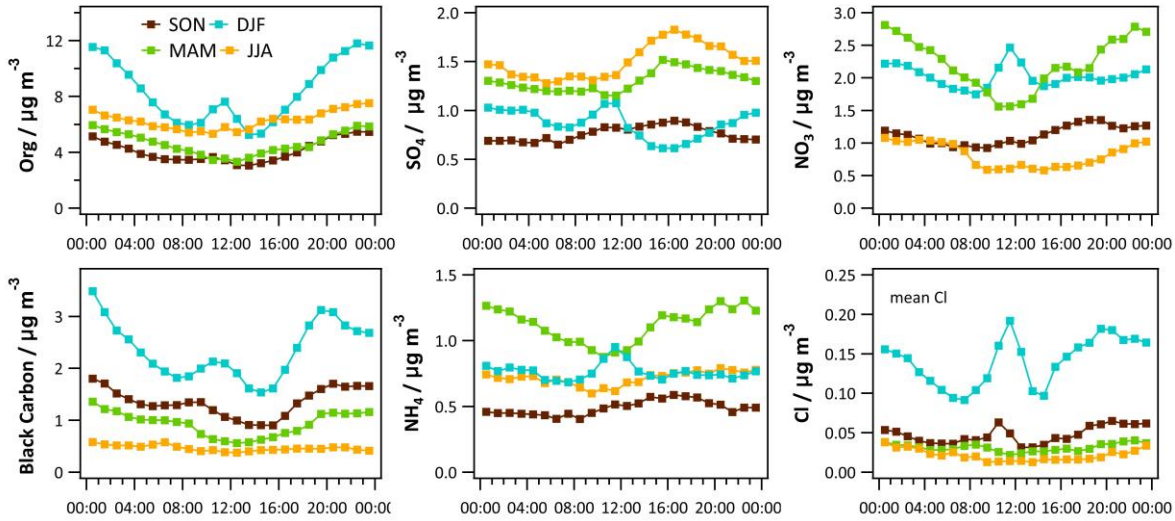

281

282 **Fig. 2** Seasonal, diurnal cycles of the measured PM_1 components (hourly averages) for the
283 organic and inorganic species (sulphate, nitrate, ammonium, and chloride) of the ACSM, and
284 equivalent black carbon.

285

286 ## 3.2 Seasonal PMF *Pre-tests*

287 The automated rolling PMF analysis requires the knowledge of the reference profiles as well
288 as the number of factors. This section presents how the number of factors was determined based
289 on seasonal PMF *pre-tests* (refer to Section 3.2.1 in the Supplement for methodology). Initially,
290 unconstrained PMF (3 to 6 factors) was performed separately for the different seasons by
291 following the SA guidelines provided by Crippa et al. (2014). Typically, the HOA profile is
292 characterised by a high contribution of alkyl fragments (*e.g. m/z* =43, *m/z* =57) and the
293 corresponding alkenyl carbocations (*e.g. m/z* = 41, *m/z* = 55), and the factor profile is relatively
294 consistent over time and different locations. The BBOA profile exhibits significant signals at

295 *m/z* = 60 and *m/z* =73, which are well-known fragments arising from fragmentation of
296 anhydrous sugars present in biomass-related emissions (Alfarra et al., 2007). The HOA profile
297 is present throughout the whole year for the unconstrained PMF runs, while the BBOA profile
298 exists for all seasons except in summer. However, as shown in **Fig. S2**, the measured fraction
299 of *m/z* = 60 during summer was above the background level of 0.3% ±0.06% for biomass
300 burning-related air masses (Aiken et al., 2009; Cubison et al., 2011; DeCarlo et al., 2008). In
301 addition, the scaled residual at *m/z* = 60 was decreased when a BBOA factor profile was
302 constrained. Thus, we decided to constrain the BBOA factor for all seasons to potentially
303 capture some local events, such as some open fires and barbeques in summer.

304 No evidence for the presence of a cooking-related OA (COA) factor was found based on the
305 seasonal pre-analysis of the key fragments (*m/z* 55 and *m/z* 57). **Figure S3** shows no difference
306 in the slope of the absolute mass concentration of *m/z* 55 vs *m/z* 57 for different hours of the
307 day (**Fig. S3a**), while different seasons show different slopes (**Fig. S3b**). Therefore, a COA
308 factor was not considered in the PMF model. Moreover, a rapid increase of the measured
309 fraction of *m/z* = 58, 84, and 98 together with *m/z* 39 (potassium signal) was observed after a
310 filament exchange on 14 April, 2014. It was likely that the ACSM's sensitivity towards those
311 ions was changed by the filament exchange. Also, this 58-OA factor was present for spring,
312 summer, and autumn in 2014 in unconstrained PMF runs all the time after the filament change.
313 Therefore, we kept this factor for these three seasons.

314 For the factor(s) with a secondary origin, we performed PMF models with a different number
315 of factors (3–6) to assess if the oxygenated OA (OOA) factor is separable without mixing with
316 primary organic aerosol (POA) factors (with a high contribution of *m/z* 44 that is likely
317 dominated by the CO_2^+ ion, derived from decomposition of carboxylic acids (Duplissy et al.,

2011)). We conducted these tests (with a different number of factors) independently for the different seasons (autumn 2013, winter, spring, summer, autumn 2014).

We analysed the winter data first by constraining an HOA factor profile (Crippa et al., 2013) with a tight *a*-value of 0.05. The 3-factor solution (with one OOA factor, i.e., less oxidized OOA (LO-OOA) and more oxidized OOA (MO-OOA)) showed similarly good agreement of HOA and BBOA with the external tracers (NO_x, eBC from traffic source (eBC_{tr}), eBC from wood burning source (eBC_{wb})) as the 4-factor solution (with two OOA factors). However, the scaled residual of *m/z* 60 was reduced for the solution with two OOA factors. Moreover, the solution with one OOA factor was not sufficient to explain the variabilities of measured f_{44} vs f_{43} (excluding the primary organic aerosol (POA) factors). For 5- and 6-factor solutions, the BBOA and LO-OOA factors started to split. Eventually, we selected the 4-factor solution (HOA, BBOA, MO-OOA, LO-OOA) as the best representation of the winter data.

After the bootstrap seasonal PMF runs of the winter data (details in Section 3.2.2 of the Supplement), we extracted the HOA and BBOA profiles to use them as the reference factor profiles (**Fig. S4**) for the *pre-tests* of other seasons. For the spring, summer, and autumn seasons, 3- to 6-factor PMF solutions were modelled separately for each season by constraining the HOA (*a*-value=0.1) and BBOA (*a*-value=0.3) profiles. For the 3-factor solution, we observed an OOA factor with some signals at *m/z* 58, 84, and 98 which we could not relate to a specific source or process. Also, the scaled residuals of variables showed significant levels for these three ions. In addition, the time series and factor profile of 58-OA were so distinct that PMF could easily resolve it. When we increased the number of OA factors from 3 to 4, a factor dominated by *m/z* 58, 84, and 98 emerged, named 58-OA. However, the OOA factor still showed slight signals at *m/z* 58, 84, and 98. An increase in the number of factors from 4 to 5 did not only result in a decrease in $\frac{Q}{Q_{exp}}$, but also in "clean" OOA factors without mixing with

the 58-OA factor. A further increase in the number of factors did not change $\frac{Q}{Q_{exp}}$ substantially (< 1%), and the sixth factor was a mathematical split of the 58-OA factor with *m/z* 58 as the dominating variable. Thus, the 5-factor PMF model was chosen as the most appropriate for the spring, summer, and autumn 2014 to be able to isolate this instrumental artifact via PMF. Note that we did not add the 58-OA factor for the autumn season in 2013 since it appeared only after the filament exchange on 14 April, 2014. This 58-OA factor was included while running PMF because of the rapid drop of the $\frac{Q}{Q_{exp}}$ from 4 to 5 factors in the PMF model, but the source of this factor will not be discussed in the manuscript.

3.3 Full-year rolling PMF analysis

Here we present the optimised time window size (14 days) (details of the time window optimisation are given in Section 4 of the Supplement and in **Fig S10**). In total, we considered 53.4% of the PMF runs (11087 out of 20750) with only 11 non-modelled data points. The results of the full-year PMF analysis of the 30-min resolved ACSM data are summarised in **Fig. 3**. The relative contributions of the OA factors are in addition shown in **Fig. 3b**. The primary traffic-related HOA had very little variation (seasonal averages between 8.1 and 10.1%) throughout the year (**Fig. 4**). In contrast, BBOA showed a distinct yearly cycle (8.3–27.4%) with a yearly averaged contribution of 17.1%. It increased significantly (to 27.4%) in winter which is typical for Alpine valleys (Szidat et al., 2007). It means that biomass burning was the most important primary OA source during the cold season in Magadino. The eBC_{wb} showed similar trends as the BBOA factor time series during the cold seasons (**Fig. 3c**). The contribution of 58-OA remained small before the filament was changed on 14 April 2014, which is expected because we could not retrieve this factor in seasonal unconstrained PMF runs before April 2014.

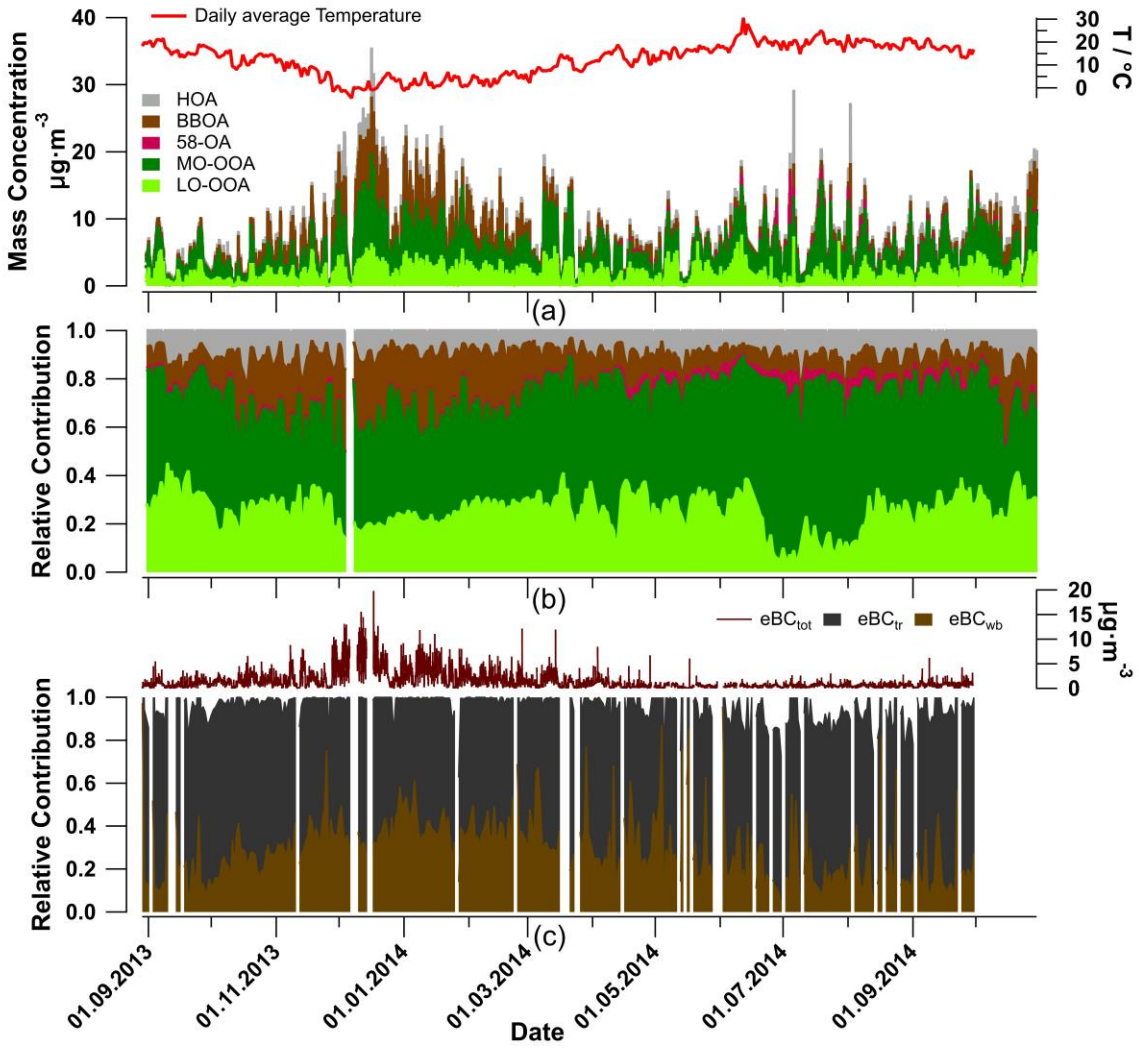

365

366 **Fig. 3** Annual cycles of OA components: (a) absolute and (b) relative OA contributions plotted

367 as 30-min resolved time series, (c) BC source apportionment.

368

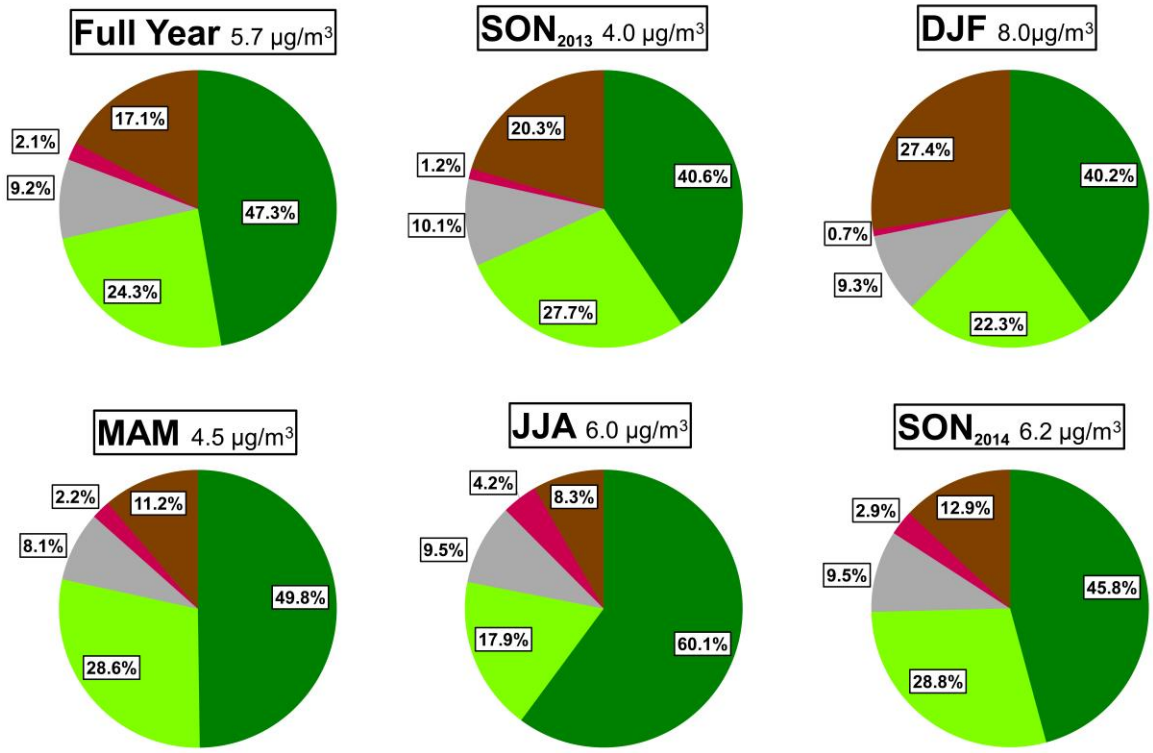

369

370 **Fig. 4** OA pie charts for the whole year and for the different seasons.

371

372 In this study, we retrieved two OOA factors, LO-OOA and MO-OOA. Total OOA (LO-
373 OOA+MO-OOA) contributed substantially to the total OA mass throughout the whole year,
374 with an average contribution of 71.6% (**Fig. 3b**; **Fig. 4**). In general, the contribution of OOA
375 to the total OA mass did not vary distinctly over the seasons but reached a maximum of 90.1%
376 on 12 June 2014, the day with the highest daily average temperature (30.7 °C).

377 In this work, we made head-to-head comparisons between the seasonal bootstrap solutions and
378 the rolling PMF results (see **Fig. A1**, **Fig. A2**, **Fig. A3**, and **Table A1** in the Appendix) in terms
379 of mass concentrations, factor profiles, scaled residuals, and correlations between time series
380 for each factor and corresponding external tracers. We found consistent factor profiles and
381 mass concentrations for the constrained factors (i.e., HOA, BBOA, and 58-OA), while OOA
382 factors showed quite some differences in both mass concentrations and factor profiles. Rolling

PMF provided slightly better correlations and smaller scaled residuals. Therefore, we consider rolling PMF results to be more environmentally reasonable than those of the seasonal PMF (more details in Appendix A).

3.3.1 Optimised OA factors retrieved from a rolling PMF model

The primary and secondary OA factors retrieved as an annual mean of all optimised PMF solutions together with their diurnal cycles for all seasons are shown in **Fig. 5**. Note that the primary factors (HOA, BBOA, and 58-OA) were constrained, where the 58-OA profile was tightly constrained with an *a*-value of 0.05 due to the uniqueness of its chemical profile, while the HOA and BBOA model profiles varied more due to looser constraints (**Fig. S8**). HOA and BBOA had averaged *a*-values of 0.207±0.036 and 0.195±0.050, respectively. In addition, they both showed good agreement with previous studies (Crippa et al., 2014; Ng et al., 2011b). The probability distribution function (PDF) of applied *a*-values for selected PMF runs vs time was also investigated (**Fig. S8**). Most selected runs chose *a*-values of 0.1–0.3 for HOA and BBOA. The OOA factors show larger variations in the chemical profiles because these two factors were not constrained due to the high variability of oxidation processes governing the secondary factors.

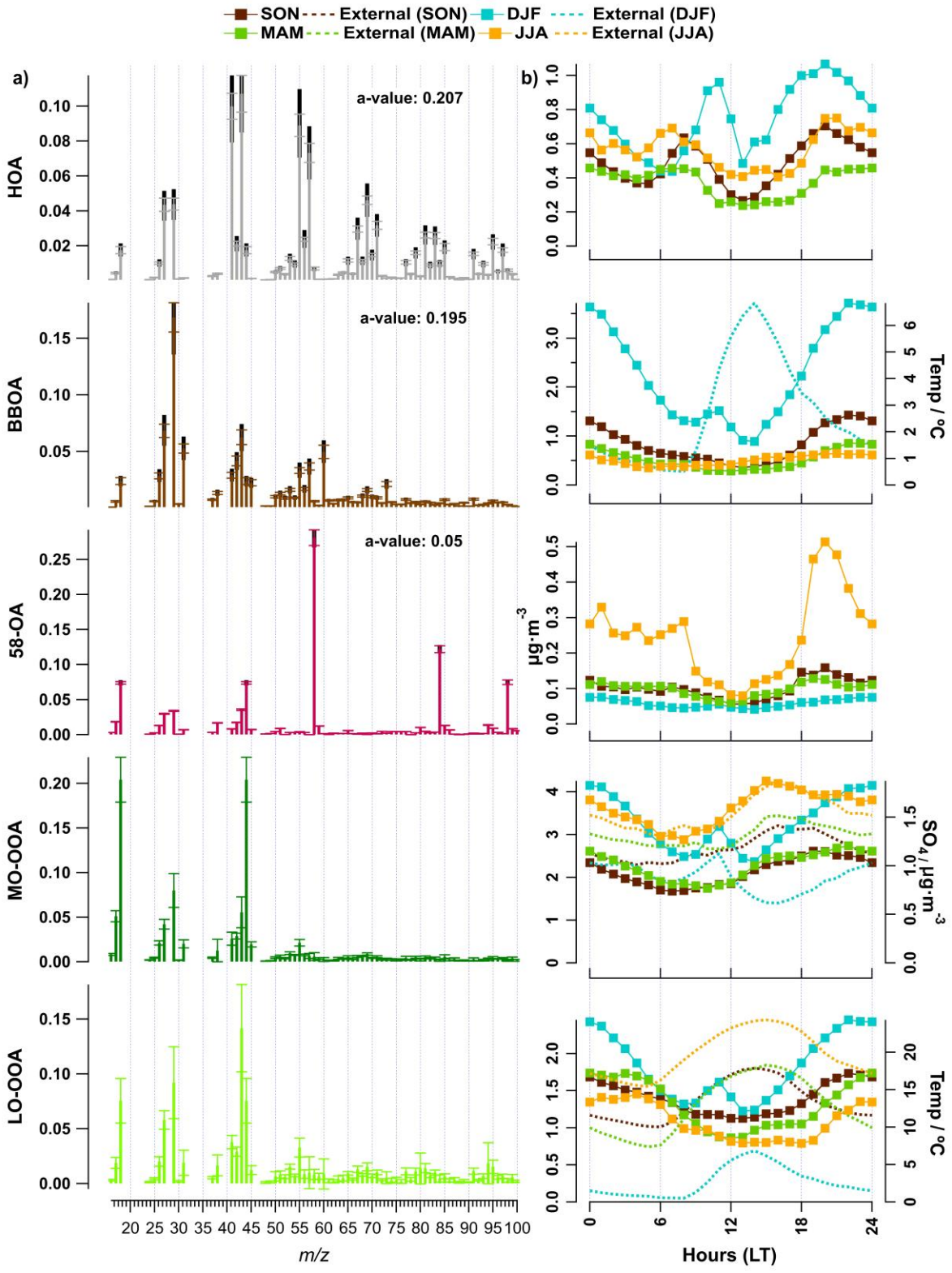

399

400 **Fig. 5** Overview of the primary and secondary OA components in Magadino in 2013-2014: (a)
401 OA factor profiles and (b) seasonal diurnal cycles of HOA, BBOA, LOA, MO-OOA, and LO-
402 OOA. The ambient temperature is shown on the LO-OOA diurnal plots. In (a) the error bar is
403 the standard deviation; the black bars show the maximum and the minimum that the variable
404 was allowed to vary from the reference profiles. The average, 10th, and 90th percentiles for a-

values of HOA are 0.195, 0.007 and 0.378, respectively. Also, the average, 10^{th}, and 90^{th} percentiles for a-values of BBOA are 0.202, 0.025 and 0.379, respectively.

Due to extensive residential wood combustion combined with winter inversions, the concentrations of BBOA and eBC_{wb} were three times higher at night than at midday. As discussed above, during winter, all of the air pollutants, including all PMF factors peaked concurrently at 10–11 a.m. (local time) due to delayed illumination of the valley site and slow wind speed near the ground (light blue markers in **Fig. 2** for total PM_1 and **Fig. 5b**). In summer, an additional local photochemical production led to an increasing MO-OOA mass during the day (red markers in **Fig. 5b**), similar to the sulphate diurnal behaviour (R^2=0.63). A nighttime increase and a daytime decrease of the LO-OOA mass during spring and summer apparently followed condensation and re-evaporation cycles of semi-volatile species, similar to the behaviour of ammonium nitrate. Additionally, nocturnal chemistry of NO_3/N_2O_5 radicals could lead to the formation of HNO_3 *via* N_2O_5 hydrolysis and of organic nitrates *via* oxidation of VOCs (Brown et al., 2004; Dentener and Crutzen, 1993), thus influencing the diurnal cycles of both particulate nitrate and LO-OOA (with R^2 = 0.48 for spring and R^2 = 0.36 for summer).

Fig. 6 also presents the diurnal cycles of HOA, eBC_{tr} and NO_x with different patterns for weekdays and weekends. The hourly averages of HOA and eBC_{tr} and the NO_x mixing ratio peak during the morning and evening rush hours over the weekdays, while on the weekends there is only an evening pollution increase coinciding with the time when people come back from holidays or nighttime leisure activities.

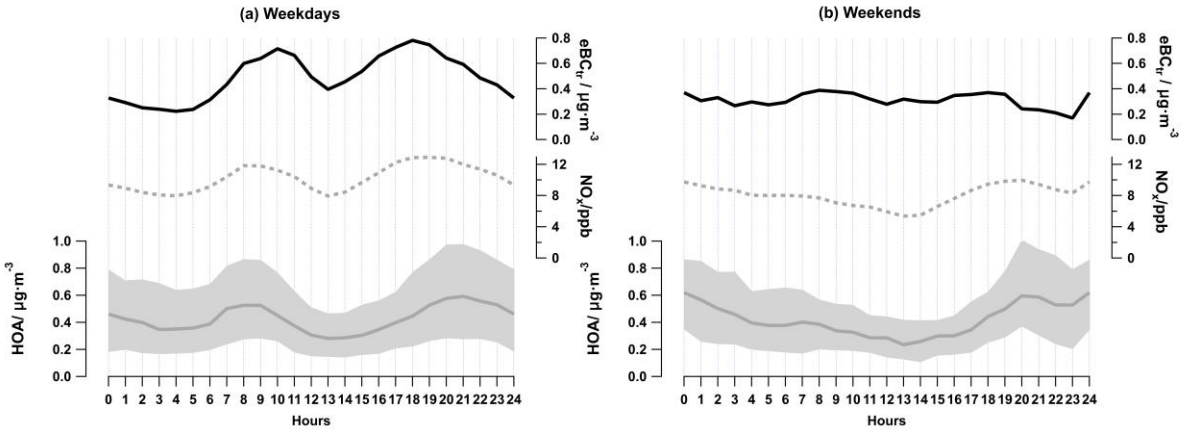

Fig. 6 Diurnal cycles of HOA (grey symbols), black carbon apportioned to traffic emissions eBC_{tr} (dashed lines) and NO_x (dotted lines) for weekdays (a) and weekends (b). The shaded areas represent the interquartile range for HOA (1-hour averages).

3.3.2 f_{44}/f_{43} analysis of secondary OA factors

While *m/z* 44 is mostly from the fragment of CO_2^+, a fingerprint of oxygenated species, *m/z* 43 can originate from $C_2H_3O^+$ (a fingerprint of semi-volatile species) or $C_3H_7^+$ (a fingerprint of the primary emissions of hydrocarbon-like species) (Canonaco et al., 2015; Chirico et al., 2010; Ng et al., 2010). Thus, f_{44} and f_{43} are often used to identify the oxidation state of the factors, which is crucial to differentiate the MO-OOA and LO-OOA factors. Under the premise that the POA factors and the 58-OA factor are all well-resolved, it is essential to investigate the relationship between the *m/z* 44 and *m/z* 43 signals in the OOA factors to determine whether or not one/two OOA factors are sufficient to explain the dataset. In addition, the shapes of the yellow-red dots shown in an f_{44} vs f_{43} plot (**Fig. 7**) may also include some source-related information. **Fig. 7** depicts the relationship between f_{44} and f_{43} of two modelled OOA factors for the different seasons. The yellow cloud of data points represents the measured f_{44} vs f_{43} after subtracting the *m/z* 44 and *m/z* 43 signals contributed by the primary HOA, BBOA and 58-OA factors (Eq. S11 and Eq. S12). They are colour coded by the total OA mass concentration (data points with OA mass concentration below 2 $\mu g \cdot m^{-3}$ are hidden).

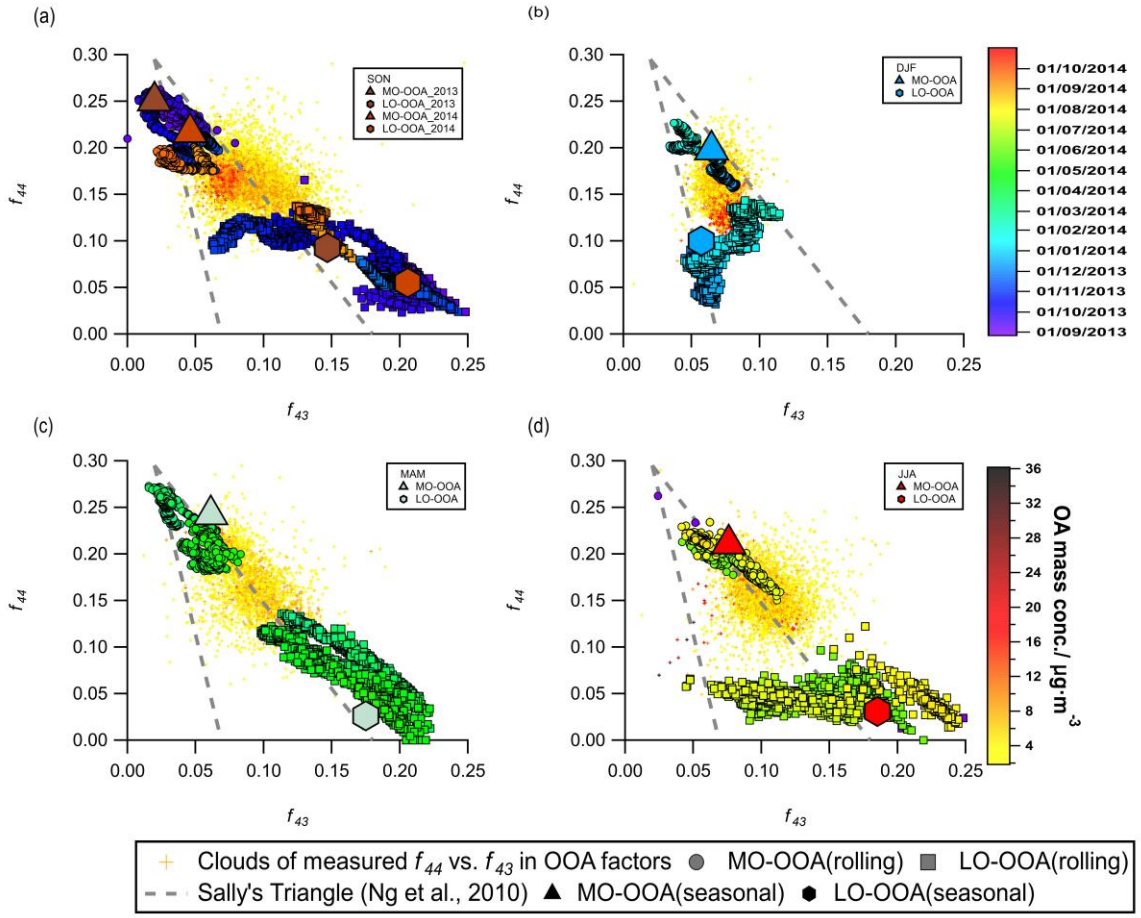

446

447 **Fig. 7** f_{44} and f_{43} of OOA (after subtraction of signals contributed by the primary HOA, BBOA
448 and 58-OA factors) for four different seasons. The small yellow/red crosses of data points
449 represent the f_{44} vs f_{43}. They are colour-coded by the total OA mass concentration. The bigger
450 size of triangles and hexagons represent the ratios between f_{44} and f_{43} intensities within the
451 factor profiles of MO-OOA and LO-OOA in seasonal solutions, respectively. The smaller size
452 of circles and squares are ratios between f_{44} and f_{43} intensities within the factor profiles of MO-
453 OOA and LO-OOA from rolling PMF analysis, which are colour-coded by date and time. The
454 dashed lines represent Sally's triangle from Ng et al., (2010) and depict the region where OOA
455 from multiple PMF analyses during the last decade resided in the f_{44} vs f_{43} space.

456

457 As shown in **Fig. 7a**, the data points in Sep–Oct (both in 2013 and 2014) were located on the
458 right side of the triangle presented first by Ng et al. (2010), while the November (2013) data
459 points were located within the triangle. In addition, the spring and summer data points (**Fig. 7c**
460 and **Fig. 7d**) were all located rather on the right side of the triangle, but the winter points lied
461 within the triangle (**Fig. 7b**). We made a similar plot but with monthly resolution and different
462 colour codes in **Fig. S9.** The data points located within the triangle correspond to the time with

a lower temperature than those that are closer to the right side of the triangle in **Fig. S9**. It could be explained by the increased biogenic OOA contributions when the temperature was higher, as biogenic OOA tends to be distributed along the right side of the triangle (Canonaco et al., 2015; Pfaffenberger et al., 2013). Also, when the temperature decreases, the increased biomass emissions make the OOA points lie vertically within the triangle (Canonaco et al., 2015; Heringa et al., 2011), which is the case for the winter data (**Fig. 7b**).

In July 2014, the rolling PMF LO-OOA moved towards the left side of the plot due to increasing influences from *m/z* 80, *m/z* 94 ($C_2H_6S_2^+$), *m/z* 95, and *m/z* 96 (**Fig. S7**). Because the OA signal of *m/z* 80 is directly calculated from *m/z* 94 (Allan et al., 2004), we did not investigate the sources of *m/z* 80. In July, a potential source of these distinct ions was some oxidation products of dimethyl disulphide, which shows signals at *m/z* 94, *m/z* 95, and *m/z* 96 (NIST Mass Spectrometry Data Center, 2014). Dimethyl disulphide is widely used in pesticides. Considering that the sampling site is in the middle of a farmland, and the diurnal variation of *m/z* 94 appeared to peak during the daytime, we considered the LO-OOA in July to be highly affected by agricultural activities. However, the static factor profiles of summer LO-OOA from the seasonal summer solution had much smaller intensities for *m/z* 80 and *m/z* 94 (**Fig. S4**), which enhanced the scaled residuals for these two variables in the seasonal solutions.

In winter, LO-OOA (**Fig. 9b**) was highly affected by biomass burning emissions characterised by the presence of *m/z* 60, 73 (Alfarra et al., 2007), and the LO-OOA position in the f_{44} vs f_{43} space moved towards the top right direction in the plot due to the increasing biogenic influence as the temperature rose (**Fig. 7b**, **Fig. S9**) (Canonaco et al., 2015).

Fig. 7 also highlights the advantages of rolling PMF over seasonal PMF due to its time-dependent source profiles. Both seasonal and rolling results show that the linear combinations of OOA factors could adequately explain most of the measured OOA points for all the seasons.

However, with the static OOA factors for seasonal PMF solutions, it remains challenging to capture the variabilities of some measured data points. In contrast, the rolling PMF OOA factors can move correspondingly with the temporal changes of the clouds, which moves the factor profiles closer to reality and potentially decreases the scaled residuals significantly (**Fig. A3**). **Figure S9** also shows the movements of LO-OOA and MO-OOA factor profiles monthly, where LO-OOA moves towards the right direction as the temperature increases, except for the two light blue squares (June and July) in **Fig. S9a**. It is clear that temperature plays an important role for the positions of LO-OOA and MO-OOA in the f_{44} vs f_{43} space due to its influences on the OOA sources (biogenic or anthropogenic) as well as the atmospheric processes, which is consistent with previous studies in Zurich (Canonaco et al., 2015).

3.3.3 Statistical and rotational uncertainties

As suggested by Canonaco et al. (2021), combining the bootstrap resampling and the random *a*-value techniques together with the rolling mechanism, we calculated the standard deviation (σ) and the mean (μ) of the mass concentration for each data point from each OA factor in selected "good" PMF runs. We estimated the uncertainty of each OA factor using the slope of the linear fit of σ vs μ. (**Fig. 8**). Since the 58-OA factor was tightly constrained with an *a*-value of 0.05, it had the smallest variability (4%). Overall, we found relatively smaller errors of HOA, BBOA, and MO-OOA (i.e., 18%, 14%, and 19%, respectively) and an error of 25% for LO-OOA, which is comparable with the previous study (Canonaco et al., 2021). The errors for both the MO-OOA and the LO-OOA factor showed some temperature dependence. However, this actually varied with time, and the errors did not significantly change when we divided the dataset into four different temperature groups. Still, data points with higher temperature tended to have larger error for the total OOA than with lower temperature (**Fig. 8f**). This was most likely due to the increase of biogenic emissions and the increasing photochemistry (high O_3

511 and NO_2 concentration) at high temperature (>20 °C), which caused the complexity of the OOA

512 sources.

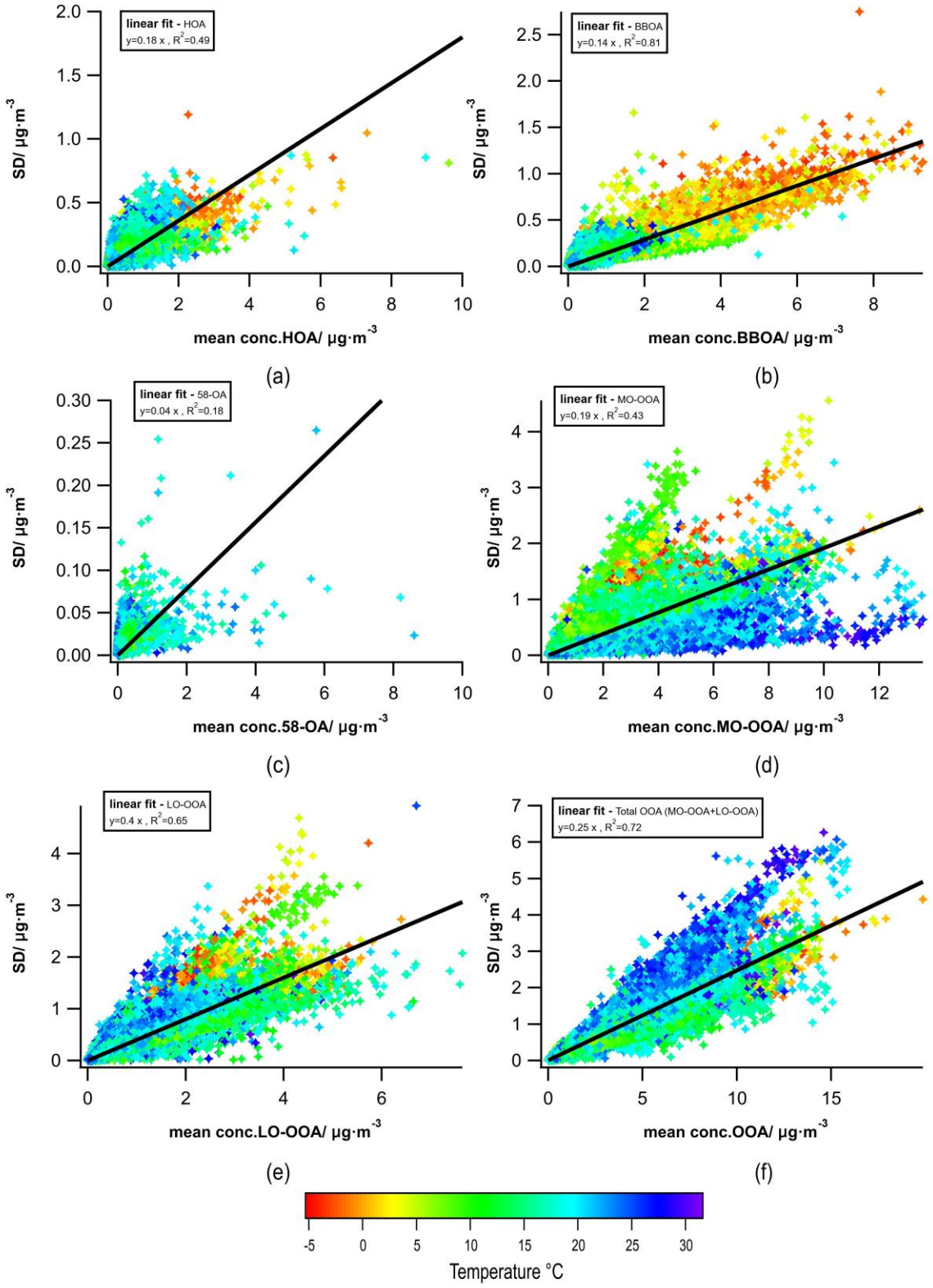

Fig. 8 Absolute statistical uncertainties of PMF for HOA, BBOA, 58-OA, LO-OOA, MO-OOA and total OOA (LO-OOA+MO-OOA) for all data. The data points are colour-coded by temperature. The PMF error (uncertainties) of selected PMF runs and rotational uncertainties are estimated using the slope of the linear regression of standard deviation (σ) vs. the averaged mass concentration (μ) for each factor.

3.3.4 Online vs. offline

The mass concentrations for HOA, BBOA and total OOA were compared with corresponding offline AMS results (Vlachou et al., 2018) (**Fig. S11**). Despite some disagreement during winter (BBOA and total OOA), BBOA showed a high correlation –with the offline results for both PM_{10} and $PM_{2.5}$, with R^2 of 0.83 and 0.84, respectively. The correlation for total OOA was somehow lower, with R^2 of 0.31 and 0.46 for the offline results of PM_{10} and $PM_{2.5}$ OOA, respectively. **Fig. 9a** shows that the rolling results had a higher OOA concentration during the winter season than the offline $PM_{2.5}/PM_{10}$ results, while the rolling results present a lower BBOA concentration during the winter season than the offline $PM_{2.5}/PM_{10}$ results (**Fig. S11b**). As shown in **Fig. 9b,** LO-OOA in the rolling results were heavily affected by biomass burning with apparent biomass trace ions (i.e., *m/z* 60 and 73). The offline results apportioned this biomass burning-affected LO-OOA to BBOA, whereas the online ACSM measurements with a higher time resolution were capable of capturing the fast oxidation process of biomass burning sources. In addition, the rolling PMF technique enabled the LO-OOA factor profile to adapt to the temporal viabilities of OA sources, so the relatively aged biomass burning OA fraction was apportioned into LO-OOA during wintertime by rolling PMF. Therefore, the offline AMS technique tended to underestimate OOA but overestimate BBOA in this study. The yellow line in **Fig. 9a** depicts the mass concentration of *m/z* 60 within LO-OOA, which clearly shows significant enhancements during winter, as well as a good agreement with the total OOA time series from the rolling results. **Figure S11** shows that HOA did not correlate at all, which is expected because HOA is typically not water-soluble, and therefore has a very low recovery rate of 0.11 for the offline AMS technique based on the Daellenbach et al. (2016).

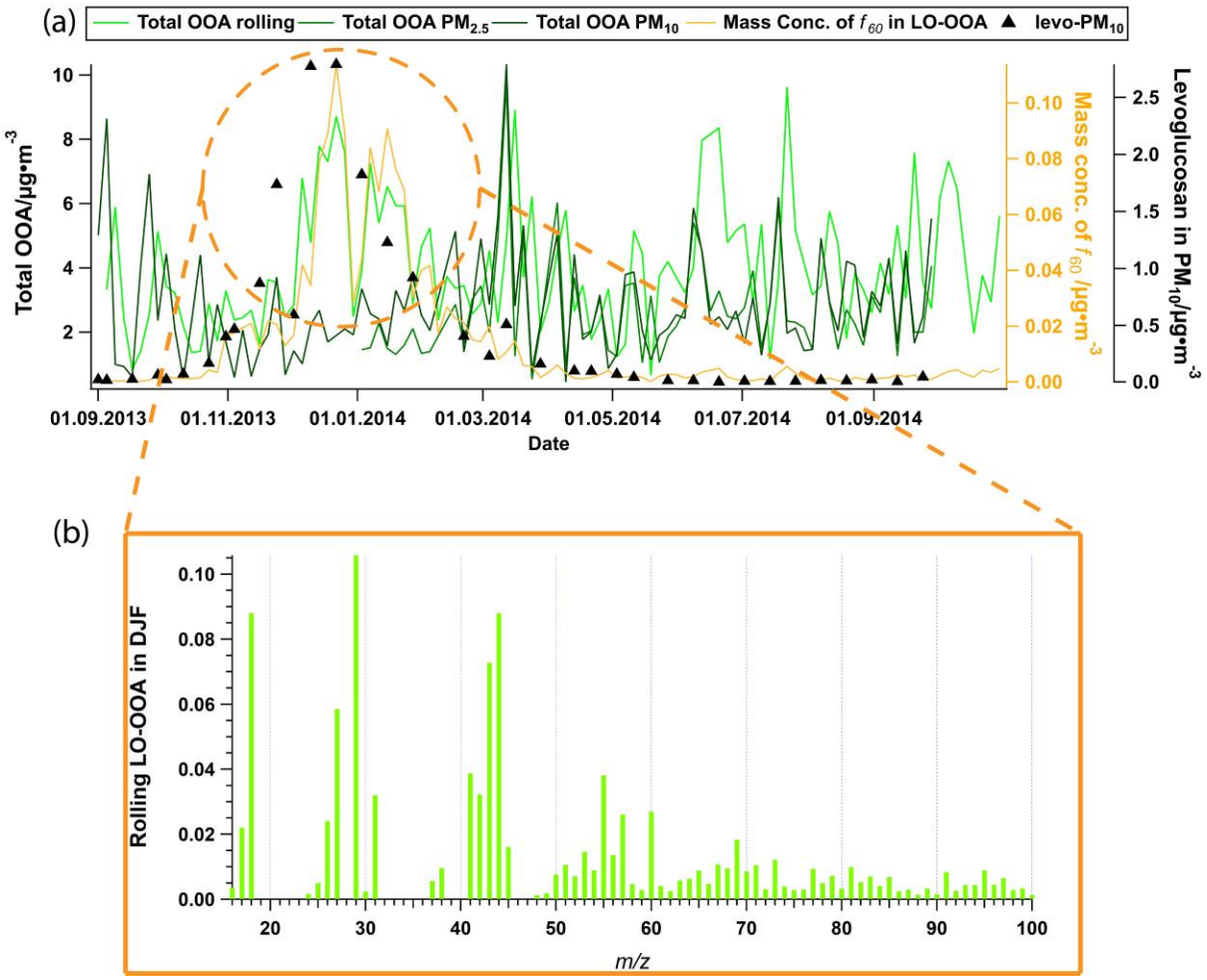

Fig. 9 (a) Time series of total oxygenated organic aerosol (LO-OOA+MO-OOA) from online and offline source apportionment solutions, together with f_{60} in LO-OOA for online solution, and levoglucosan in PM_{10} filters; (b) Averaged LO-OOA factor profile from the online solution during DJF (Dec, Jan, and Feb), when online total OOA is significantly higher than that of the offline solution.

4 Conclusions

In this study, we conducted the first rolling PMF analysis on a 13-month ACSM data collected at a rural site in Switzerland. With the help of the small rolling PMF time window and the random *a*-value and bootstrap resampling analysis, we obtained a time dependent SA result with error estimations. Overall, we resolved a comprehensive 5-factor solution with HOA, BBOA, 58-OA, MO-OOA, and LO-OOA. The contribution of HOA was constant during the

555 year (8.1–10.1%), while BBOA showed a clear seasonal variation (8.3–27.4%), which peaked
556 during winter (due to an increased residential heating source) and contributed least in summer.
557 OOA was a dominant source throughout the year, with a contribution of 71.6% on a yearly
558 average. However, the biomass burning source had a strong influence on LO-OOA formation
559 in winter. Together with BBOA, they make residential heating a considerable source at
560 Magadino during winter. Therefore, mitigation of residential wood combustion should be
561 considered to reduce PM levels in Magadino and similar locations, especially in winter.

562 This manuscript also provided a recommended criterion list (**Table S1**) and a novel way to
563 define thresholds with minimum subjective judgements (student's *t*-test), which could be a
564 leading example for other SoFi Pro users to conduct rolling PMF. To ensure a good
565 representation of the modelled POA factors and to validate the SA results, we also used the
566 correlations between the PMF factor time series and external data. Both HOA and BBOA
567 agreed well with the corresponding external tracers (NO_x, eBC_{tr}, and eBC_{wb}) for the yearly
568 cycles, except for summer. This is because the aethalometer model for eBC SA has higher
569 uncertainties with smaller eBC_{wb} mass concentrations. Also, NO_x could originate from multiple
570 sources in this season. Therefore, we used HOA vs eBC and $EV_{60,BBOA}$ to justify these two
571 factors in summer. The correlation of HOA vs eBC had an R^2 of 0.28, with an $EV_{60,BBOA}$ of
572 0.55 in summer. Moreover, the MO-OOA and LO-OOA factors were well correlated with
573 inorganic SO_4 and NO_3, respectively. The identified primary and secondary OA factor profiles
574 were consistent with the OA factors previously found at various urban, rural, and remote
575 European locations.

576 This paper assessed the statistical and rotational uncertainties of the PMF solution by
577 combining the bootstrap resampling technique and the random *a*-value approach. It shows

relatively small errors for constrained factors compared with a previous study in Zurich (Canonaco et al., 2021) and comparable errors for the OOA factors.

We also presented a head-to-head comparison between seasonal PMF solutions and the rolling PMF solution. The POA factors showed good agreement between seasonal and rolling PMF solution, while the OOA factors exhibited greater differences. Overall, the rolling PMF provided slightly better agreements with external tracers, especially between the OOA factors and corresponding inorganic salts. In addition, the rolling PMF results provided a better representation of the measurements by adapting the temporal variations of OOA factors in the f_{44} vs f_{43} space, which also led to much smaller scaled residuals than for the seasonal PMF. Therefore, the rolling PMF is highly useful when the user wishes to better separate OOA factors (especially during cold seasons) and better represent the measurements. In addition, we will also recommend using the rolling PMF to facilitate the analysis of long-term trends of OA sources with some prior knowledge of OA sources. However, it remains challenging to objectively define the transition point to an improved source apportionment for rolling PMF analysis when a different number of OA factors is necessary for different periods. An upcoming manuscript (Via et al., in prep.) will present more details of the comparison between rolling and seasonal results for multiple datasets. The time series of BBOA and total OOA agreed well with those from offline AMS SA results (Vlachou et al., 2018), except for winter when the offline AMS technique did not capture the fast oxidation processes of biomass burning emissions.

Knowledge of diurnal, seasonal and annual changes in OA sources is essential for interpreting the yearly cycles of OA and defining mitigation strategies for air quality. With the help of more accurate and realistic OA sources together with an estimation of the statistical uncertainty of PMF, more constraints can be provided both for climate and air quality models. These

improved results are therefore highly valuable for policymakers to solve aerosol-related environmental issues.

5 Appendix A: Comparison between seasonal and rolling PMF solutions

The bootstrapped seasonal PMF solutions were compared with the full-year rolling PMF results as follows. The correlations with external data, the ion intensities in the factor profiles and the mass concentrations retrieved from the two different source apportionment techniques were compared for each factor. The correlations of the factor time series with external data (i.e., NO_x, eBC_{tr}, eBC_{wb}, eBC_{totoal}, SO_4, NO_3, and NH_4) are presented in **Table A1**. The rolling results generally showed slightly better correlations between LO-OOA and NO_3, MO-OOA and SO_4, and total OOA with NH_4 than the seasonal PMF results, which is consistent with the comparison results from Canonaco et al. (2021). A significant improvement was evident for LO-OOA vs NO_3 in spring (with R^2 increasing from 0.02 to 0.48). Concerning the correlations of POA factors with external data, rolling results and seasonal showed similar results

Table A1 Correlation coefficients ($R^2_{pearson}$) between the factor contributions and expected tracers over the year and for individual meteorological seasons ($p<0.05$).

Factor	Yearly		SON_2013		DJF		MAM		JJA		SON_2014	
	Seasonal	Rolling	Seasonal	Rolling	Seasonal	Rolling	Seasonal	Rolling	Seasonal	Rolling	Seasonal	Rolling
HOA / NO_x	0.37	0.35	0.52	0.5	0.46	0.47	0.34	0.36	0.15	0.15	0.44	0.42
HOA / eBC_{tr}	0.34	0.33	0.29	0.35	0.41	0.42	0.39	0.31	N/A	N/A	0.38	0.39
HOA / eBC	0.55	0.51	0.79	0.77	0.77	0.73	0.5	0.41	0.29	0.28	0.5	0.47
BBOA / eBC_{wb}	0.82	0.82	0.81	0.79	0.84	0.81	0.67	0.6	N/A	N/A	0.3	0.27
MO-OOA / SO_4^{2-}	0.58	0.49	0.49	0.61	0.52	0.49	0.62	0.66	0.63	0.57	0.43	0.46
LO-OOA / NO_3^-	0.11	0.32	0.28	0.42	0.28	0.23	0.02	0.48	0.33	0.36	0.19	0.29
OOA/ NH_4^+	0.46	0.44	0.52	0.55	0.34	0.26	0.73	0.75	0.48	0.47	0.57	0.59

Fig. A1 showed a good agreement for two techniques, except for MO-OOA and LO-OOA. In general, the slope of 1.09 for rolling total OOA vs seasonal OOA suggests a slight underestimation of the OOA contribution by the seasonal PMF solutions, while the slope (<1) for HOA and BBOA suggests that the seasonal PMF solutions overestimate HOA and BBOA.

In addition, 58-OA shows the best agreement between the seasonal and rolling solutions due to the tight constraint of 58-OA with an *a*-value of 0.05.

The LO-OOA and MO-OOA factors showed worse agreement than the POA factors for the whole dataset. They had good correlations in each meteorological season, however, with different slopes. For instance, seasonal PMF underestimated LO-OOA in spring and fall 2014, but both seasons showed a high correlation with rather narrow scattering. The underestimation of LO-OOA by seasonal PMF was compensated by the overestimation of MO-OOA for these two seasons, therefore, the summed OOA still showed a high correlation between rolling and seasonal PMF results. This is expected, as the rolling PMF allows the source profiles to adapt to temporal variations, while seasonal PMF only has static source profiles.

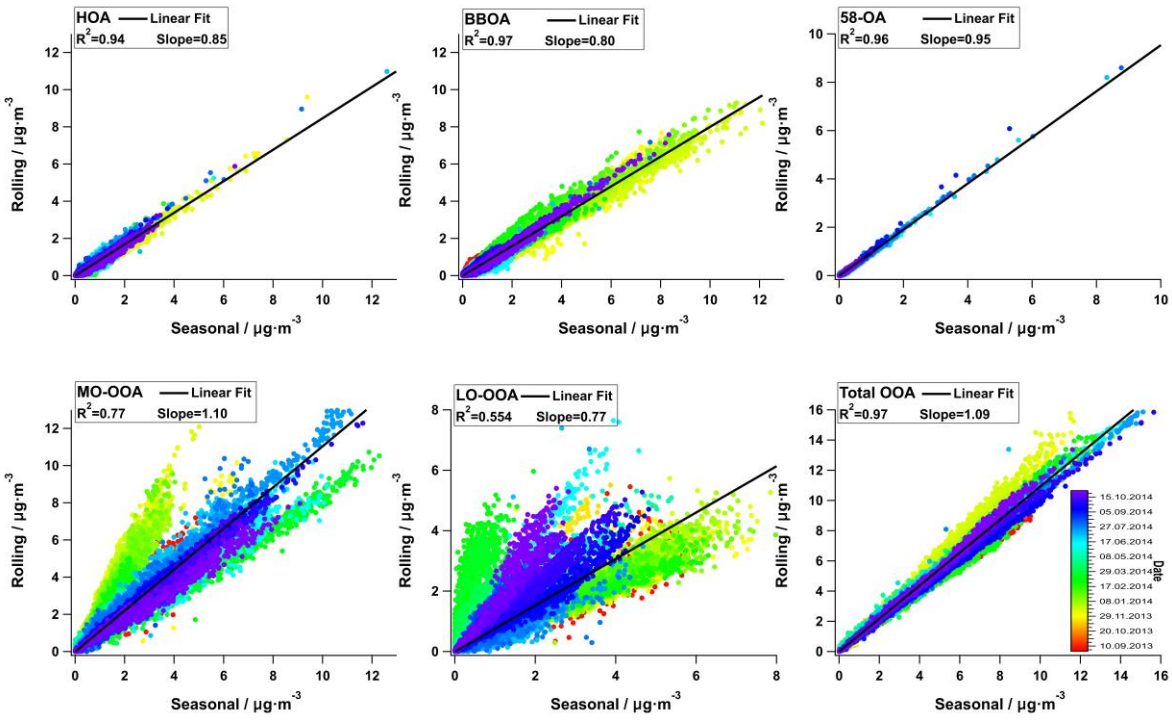

Fig. A1 Comparison of the mass concentrations resulting from rolling PMF and from the seasonal analysis for each factor (colour coded by date and time).

The differences in the major variables of the OOA factors (i.e., *m/z* 44, 43, and 60) shifted the mass concentrations significantly. Therefore, we also compared the factor profiles for both techniques (**Fig. A2**). For instance, LO-OOA during spring showed higher intensity at *m/z* 44 for the rolling PMF results than for the seasonal PMF results (**Fig. A2**), which caused the underestimation of LO-OOA for the seasonal PMF in spring. When we averaged the total OOA factor using mass-weighted MO-OOA and LO-OOA factors, rolling PMF yielded higher *m/z* 60 for all seasons. As a result, seasonal PMF slightly underestimated the summed OOA factors by around 9% but slightly overestimated the POA factors by less than <6%.

The profiles of the constrained factors (HOA, BBOA, 58-OA) from the rolling results show very high correlation with the seasonal results (**Fig. A2**), which suggests that the primary factors and the tightly constrained factor (58-OA) were consistent with the static profiles from the seasonal PMF analysis.

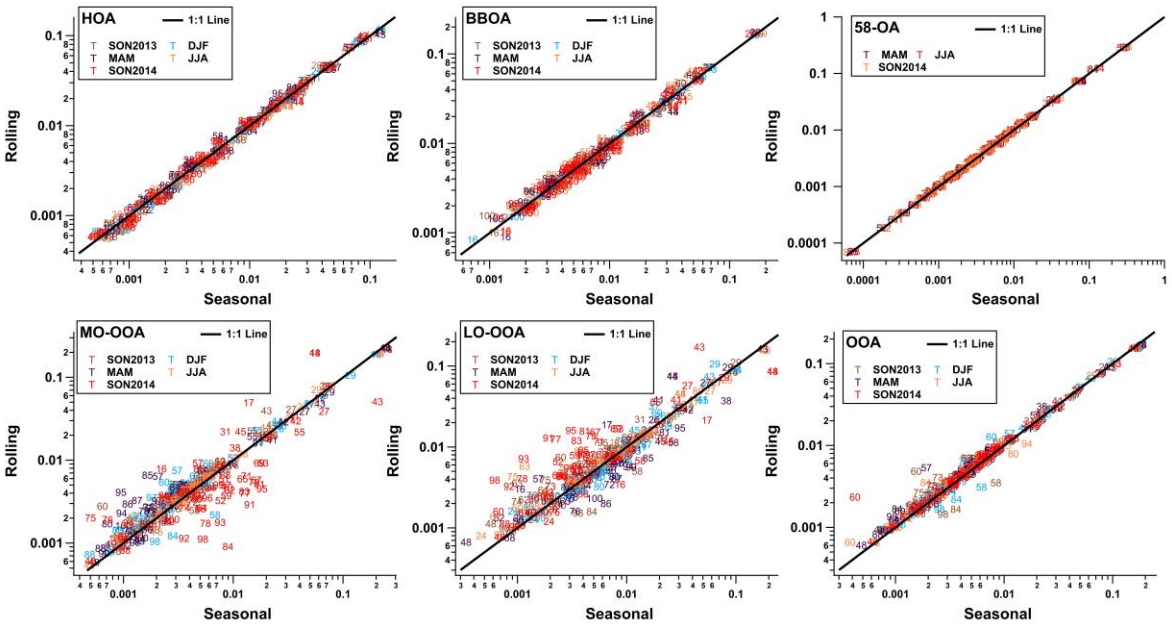

Fig. A2 Profile comparisons between rolling results and seasonal results for each factor (log scale).

We compared the scaled residuals from both source apportionment techniques (**Fig. A3**). The rolling PMF solution had smaller scaled residuals (narrower histogram and the centre was closer to 0) than that of the seasonal PMF solution, which is expected because rolling PMF had more flexibility to adapt to the temporal variabilities of the OA sources.

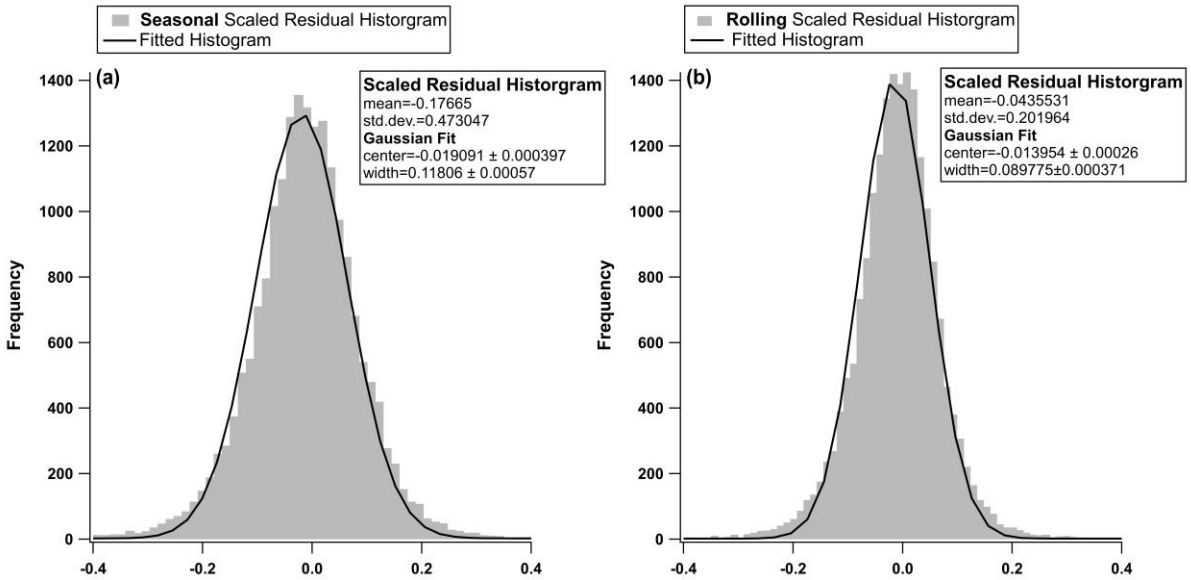

Fig. A3 Distribution of the scaled residuals over the whole year for the seasonal solution (a) and the rolling solution (b).

Summarising, HOA and BBOA were consistent for rolling and seasonal PMF analysis in terms of the time series, correlations with external tracers, and factor profiles due to the consistency of their chemical factor profiles. In contrast, the MO-OOA and LO-OOA factors were more scattered in averaged factor profiles and mass concentration, suggesting that seasonal PMF analysis was not sufficient to capture these temporal variabilities of their oxidation processes. Also, rolling PMF showed smaller scaled residuals. Therefore, we conclude that the rolling PMF analysis provides more realistic results than the seasonal analysis.

Data Availability

Data related to this manuscript are available at https://zenodo.org/record/5113896 (Chen et al., 2021).

Competing interests

Y. S., F. C., A. T. K., C. B. are working for Datalystica Ltd., the company that developed the SoFi Pro software. All authors declare no competing interests in any form for this work.

Author contributions

G. C. analysed the ACSM and BC data, then performed the rolling source apportionment and wrote the manuscript. Y. S. wrote the preliminary manuscript and analysed preliminary results. G. C., Y. S., F. C., A. T., K. R. D., J. G. S., I. EI. H., U. B., and A. S. H. P. helped editing and reviewing the manuscript. Y. S, R. F. and P. G. helped to run the campaign. P. G., and C. H. provided external data to validate PMF solution. F.C. provided technique support for SoFi Pro. F.C., A. T., K. R. D., A. V., J. G. S., I. EI. H., U. B., and A. S. H. P. participated in discussions for this study.

Acknowledgements

The ACSM measurements were supported by the Swiss Federal Office for the Environment (FOEN). The leading role of the Environmental group of the Swiss Federal Laboratories for Materials and Testing (Empa) in supporting the measurements is very much appreciated. Y. S. acknowledges supports by the “Wiedereinsteigerinnen Program” at the Paul Scherrer Institute. This study was also supported by the cost action of Chemical On-Line cOmpoSition and Source Apportionment of fine aerosol (COLOSSAL, CA16109), a COST related project of the Swiss National Science Foundation, Source apportionment using long-term Aerosol Mass

694 Spectrometry and Aethalometer Measurements (SAMSAM, IZCOZ0_177063), as well as the
695 EU Horizon 2020 Framework Programme via the ERA-PLANET project SMURBS (grant
696 agreement no. 689443).

697 References

698 Aiken, A. C., Salcedo, D., Cubison, M. J., Huffman, J. A., DeCarlo, P. F., Ulbrich, I. M.,
699 Docherty, K. S., Sueper, D., Kimmel, J. R., Worsnop, D. R., Trimborn, A., Northway, M.,
700 Stone, E. A., Schauer, J. J., Volkamer, R. M., Fortner, E., de Foy, B., Wang, J., Laskin, A.,
701 Shutthanandan, V., Zheng, J., Zhang, R., Gaffney, J., Marley, N. A., Paredes-Miranda, G.,
702 Arnott, W. P., Molina, L. T., Sosa, G. and Jimenez, J. L.: Mexico City aerosol analysis during
703 MILAGRO using high resolution aerosol mass spectrometry at the urban supersite (T0) – Part
704 1: Fine particle composition and organic source apportionment, Atmos. Chem. Phys., 9(17),
705 6633–6653, doi:10.5194/acp-9-6633-2009, 2009.

706 Alfarra, M. R., Prevot, A. S. H., Szidat, S., Sandradewi, J., Weimer, S., Lanz, V. A., Schreiber,
707 D., Mohr, M. and Baltensperger, U.: Identification of the Mass Spectral Signature of Organic
708 Aerosols from Wood Burning Emissions, Environ. Sci. Technol., 41(16), 5770–5777,
709 doi:10.1021/es062289b, 2007.

710 Allan, J. D., Delia, A. E., Coe, H., Bower, K. N., Alfarra, M. R. R., Jimenez, J. L., Middlebrook,
711 A. M., Drewnick, F., Onasch, T. B., Canagaratna, M. R., Jayne, J. T. and Worsnop, D. R.: A
712 generalised method for the extraction of chemically resolved mass spectra from Aerodyne
713 aerosol mass spectrometer data, J. Aerosol Sci., 35(7), 909–922,
714 doi:10.1016/j.jaerosci.2004.02.007, 2004.

715 Bressi, M., Cavalli, F., Belis, C. A., Putaud, J.-P. P., Fröhlich, R., Martins dos Santos, S.,
716 Petralia, E., Prévôt, A. S. H. H., Berico, M., Malaguti, A. and Canonaco, F.: Variations in the

717 chemical composition of the submicron aerosol and in the sources of the organic fraction at a
718 regional background site of the Po Valley (Italy), Atmos. Chem. Phys., 16(20), 12875–12896,
719 doi:10.5194/acp-16-12875-2016, 2016.

720 Brown, S. S., Dibb, J. E., Stark, H., Aldener, M., Vozella, M., Whitlow, S., Williams, E. J.,
721 Lerner, B. M., Jakoubek, R., Middlebrook, A. M., DeGouw, J. A., Warneke, C., Goldan, P. D.,
722 Kuster, W. C., Angevine, W. M., Sueper, D. T., Quinn, P. K., Bates, T. S., Meagher, J. F.,
723 Fehsenfeld, F. C. and Ravishankara, A. R.: Nighttime removal of NO x in the summer marine
724 boundary layer, Geophys. Res. Lett., 31(7), n/a-n/a, doi:10.1029/2004GL019412, 2004.

725 Canagaratna, M. R., Jayne, J. T., Jimenez, J. L., Allan, J. D., Alfarra, M. R., Zhang, Q., Onasch,
726 T. B., Drewnick, F., Coe, H., Middlebrook, A., Delia, A., Williams, L. R., Trimborn, A. M.,
727 Northway, M. J., DeCarlo, P. F., Kolb, C. E., Davidovits, P. and Worsnop, D. R.: Chemical
728 and microphysical characterization of ambient aerosols with the aerodyne aerosol mass
729 spectrometer, Mass Spectrom. Rev., 26(2), 185–222, doi:10.1002/mas.20115, 2007.

730 Canonaco, F., Crippa, M., Slowik, J. G., Baltensperger, U. and Prévôt, A. S. H. H.: SoFi, an
731 IGOR-based interface for the efficient use of the generalized multilinear engine (ME-2) for the
732 source apportionment: ME-2 application to aerosol mass spectrometer data, Atmos. Meas.
733 Tech., 6(12), 3649–3661, doi:10.5194/amt-6-3649-2013, 2013.

734 Canonaco, F., Slowik, J. G., Baltensperger, U. and Prévôt, A. S. H.: Seasonal differences in
735 oxygenated organic aerosol composition: implications for emissions sources and factor
736 analysis, Atmos. Chem. Phys., 15(12), 6993–7002, doi:10.5194/acp-15-6993-2015, 2015.

737 Canonaco, F., Tobler, A., Chen, G., Sosedova, Y., Slowik, J. G. G., Bozzetti, C., Daellenbach,
738 K. R., El Haddad, I., Crippa, M., Huang, R.-J., Furger, M., Baltensperger, U., Prévôt, A. S. H.,
739 Kaspar Rudolf Haddad, I. E. D., Crippa, M., Huang, R.-J., Furger, M., Baltensperger, U.,

Prevot, A. S. H., Daellenbach, Kaspar Rudolf Haddad, I. El, Crippa, M., Huang, R.-J., Furger, M., Baltensperger, U. and Prevot, A. S. H.: A new method for long-term source apportionment with time-dependent factor profiles and uncertainty assessment using SoFi Pro: application to 1 year of organic aerosol data, Atmos. Meas. Tech., 14(2), 923–943, doi:10.5194/amt-14-923-2021, 2021.

Chirico, R., DeCarlo, P. F., Heringa, M. F., Tritscher, T., Richter, R., Prévôt, A. S. H., Dommen, J., Weingartner, E., Wehrle, G., Gysel, M., Laborde, M. and Baltensperger, U.: Impact of aftertreatment devices on primary emissions and secondary organic aerosol formation potential from in-use diesel vehicles: results from smog chamber experiments, Atmos. Chem. Phys., 10(23), 11545–11563, doi:10.5194/acp-10-11545-2010, 2010.

Chow, J. C., Bachmann, J. D., Wierman, S. S. G., Mathai, C. V., Malm, W. C., White, W. H., Mueller, P. K., Kumar, N. and Watson, J. G.: Visibility: Science and Regulation, J. Air Waste Manage. Assoc., 52(9), 973–999, doi:10.1080/10473289.2002.10470844, 2002.

Crippa, M., DeCarlo, P. F., Slowik, J. G., Mohr, C., Heringa, M. F., Chirico, R., Poulain, L., Freutel, F., Sciare, J., Cozic, J., Di Marco, C. F., Elsasser, M., Nicolas, J. B., Marchand, N., Abidi, E., Wiedensohler, A., Drewnick, F., Schneider, J., Borrmann, S., Nemitz, E., Zimmermann, R., Jaffrezo, J.-L., Prévôt, A. S. H. and Baltensperger, U.: Wintertime aerosol chemical composition and source apportionment of the organic fraction in the metropolitan area of Paris, Atmos. Chem. Phys., 13(2), 961–981, doi:10.5194/acp-13-961-2013, 2013.

Crippa, M., Canonaco, F., Lanz, V. A., Äijälä, M., Allan, J. D., Carbone, S., Capes, G., Ceburnis, D., Dall'Osto, M., Day, D. A., DeCarlo, P. F., Ehn, M., Eriksson, A., Freney, E., Hildebrandt Ruiz, L., Hillamo, R., Jimenez, J. L., Junninen, H., Kiendler-Scharr, A., Kortelainen, A.-M. M., Kulmala, M., Laaksonen, A., Mensah, A. A., Mohr, C., Nemitz, E., O'Dowd, C., Ovadnevaite, J., Pandis, S. N., Petäjä, T., Poulain, L., Saarikoski, S.,

764 Sellegri, K., Swietlicki, E., Tiitta, P., Worsnop, D. R., Baltensperger, U., Prévôt, A. S. H. H.,
765 Dall'Osto, M., Day, D. A., DeCarlo, P. F., Ehn, M., Eriksson, A., Freney, E., Hildebrandt Ruiz,
766 L., Hillamo, R., Jimenez, J. L., Junninen, H., Kiendler-Scharr, A., Kortelainen, A.-M. M.,
767 Kulmala, M., Laaksonen, A., Mensah, A. A., Mohr, C., Nemitz, E., O'Dowd, C., Ovadnevaite,
768 J., Pandis, S. N., Petäjä, T., Poulain, L., Saarikoski, S., Sellegri, K., Swietlicki, E., Tiitta, P.,
769 Worsnop, D. R., Baltensperger, U. and Prévôt, A. S. H. H.: Organic aerosol components
770 derived from 25 AMS data sets across Europe using a consistent ME-2 based source
771 apportionment approach, Atmos. Chem. Phys., 14(12), 6159–6176, doi:10.5194/acp-14-6159-
772 2014, 2014.

773 Cubison, M. J. J., Ortega, A. M. M., Hayes, P. L. L., Farmer, D. K. K., Day, D., Lechner, M.
774 J. J., Brune, W. H. H., Apel, E., Diskin, G. S., Fisher, J. A., Fuelberg, H. E., Hecobian, A.,
775 Knapp, D. J., Mikoviny, T., Riemer, D., Sachse, G. W., Sessions, W., Weber, R. J., Weinheimer,
776 A. J., Wisthaler, A. and Jimenez, J. L.: Effects of aging on organic aerosol from open biomass
777 burning smoke in aircraft and laboratory studies, Atmos. Chem. Phys., 11(23), 12049–12064,
778 doi:www.atmos-chem-phys.net/11/12049/2011/, 2011.

779 Daellenbach, K. R., Bozzetti, C., Křepelová, A., Canonaco, F., Wolf, R., Zotter, P., Fermo, P.,
780 Crippa, M., Slowik, J. G., Sosedova, Y., Zhang, Y., Huang, R.-J. J., Poulain, L., Szidat, S.,
781 Baltensperger, U., El Haddad, I. and Prévôt, A. S. H. H.: Characterization and source
782 apportionment of organic aerosol using offline aerosol mass spectrometry, Atmos. Meas. Tech.,
783 9(1), 23–39, doi:10.5194/amt-9-23-2016, 2016.

784 Daellenbach, K. R., Uzu, G., Jiang, J., Cassagnes, L.-E., Leni, Z., Vlachou, A., Stefenelli, G.,
785 Canonaco, F., Weber, S., Segers, A., Kuenen, J. J. P., Schaap, M., Favez, O., Albinet, A.,
786 Aksoyoglu, S., Dommen, J., Baltensperger, U., Geiser, M., El Haddad, I., Jaffrezo, J.-L. and
787 Prévôt, A. S. H.: Sources of particulate-matter air pollution and its oxidative potential in Europe,

Nature, 587(7834), 414–419, doi:10.1038/s41586-020-2902-8, 2020.

DeCarlo, P. F., Dunlea, E. J., Kimmel, J. R., Aiken, A. C., Sueper, D., Crounse, J., Wennberg, P. O., Emmons, L., Shinozuka, Y., Clarke, A., Zhou, J., Tomlinson, J., Collins, D. R., Knapp, D., Weinheimer, A. J., Montzka, D. D., Campos, T. and Jimenez, J. L.: Fast airborne aerosol size and chemistry measurements above Mexico City and Central Mexico during the MILAGRO campaign, Atmos. Chem. Phys., 8(14), 4027–4048, doi:10.5194/acp-8-4027-2008, 2008.

Dentener, F. J. and Crutzen, P. J.: Reaction of N 2 O 5 on tropospheric aerosols: Impact on the global distributions of NO x , O 3 , and OH, J. Geophys. Res. Atmos., 98(D4), 7149–7163, doi:10.1029/92JD02979, 1993.

Dockery, D. W. and Pope, C. A.: Acute Respiratory Effects of Particulate Air Pollution, Annu. Rev. Public Health, 15(1), 107–132, doi:10.1146/annurev.pu.15.050194.000543, 1994.

Duplissy, J., DeCarlo, P. F., Dommen, J., Alfarra, M. R., Metzger, A., Barmpadimos, I., Prevot, A. S. H., Weingartner, E., Tritscher, T., Gysel, M., Aiken, A. C., Jimenez, J. L., Canagaratna, M. R., Worsnop, D. R., Collins, D. R., Tomlinson, J. and Baltensperger, U.: Relating hygroscopicity and composition of organic aerosol particulate matter, Atmos. Chem. Phys., 11(3), 1155–1165, doi:10.5194/acp-11-1155-2011, 2011.

Efron, B.: Bootstrap Methods: Another Look at the Jackknife, Ann. Stat., 7(1), 1–26 [online] Available from: https://www.jstor.org/stable/2958830, 1979.

Fröhlich, R., Cubison, M. J., Slowik, J. G., Bukowiecki, N., Prévôt, A. S. H. H., Baltensperger, U., Schneider, J., Kimmel, J. R., Gonin, M., Rohner, U., Worsnop, D. R. and Jayne, J. T.: The ToF-ACSM: a portable aerosol chemical speciation monitor with TOFMS detection, Atmos. Meas. Tech., 6(11), 3225–3241, doi:10.5194/amt-6-3225-2013, 2013.

Fröhlich, R., Crenn, V., Setyan, A., Belis, C. A., Canonaco, F., Favez, O., Riffault, V., Slowik, J. G., Aas, W., Aijälä, M., Alastuey, A., Artiñano, B., Bonnaire, N., Bozzetti, C., Bressi, M., Carbone, C., Coz, E., Croteau, P. L., Cubison, M. J., Esser-Gietl, J. K., Green, D. C., Gros, V., Heikkinen, L., Herrmann, H., Jayne, J. T., Lunder, C. R., Minguillón, M. C., Močnik, G., O'Dowd, C. D., Ovadnevaite, J., Petralia, E., Poulain, L., Priestman, M., Ripoll, A., Sarda-Estève, R., Wiedensohler, A., Baltensperger, U., Sciare, J., Prévôt, A. S. H., O'Dowd, C. D., Ovadnevaite, J., Petralia, E., Poulain, L., Priestman, M., Ripoll, A., Sarda-Estève, R., Wiedensohler, A., Baltensperger, U., Sciare, J., Prévôt, A. S. H., O'Dowd, C. D., Ovadnevaite, J., Petralia, E., Poulain, L., Priestman, M., Ripoll, A., Sarda-Estève, R., Wiedensohler, A., Baltensperger, U., Sciare, J. and Prévôt, A. S. H.: ACTRIS ACSM intercomparison – Part 2: Intercomparison of ME-2 organic source apportionment results from 15 individual, co-located aerosol mass spectrometers, Atmos. Meas. Tech., 8(6), 2555–2576, doi:10.5194/amt-8-2555-2015, 2015.

Heringa, M. F., DeCarlo, P. F., Chirico, R., Tritscher, T., Dommen, J., Weingartner, E., Richter, R., Wehrle, G., Prévôt, A. S. H. and Baltensperger, U.: Investigations of primary and secondary particulate matter of different wood combustion appliances with a high-resolution time-of-flight aerosol mass spectrometer, Atmos. Chem. Phys., 11(12), 5945–5957, doi:10.5194/acp-11-5945-2011, 2011.

Hildebrandt, L., Kostenidou, E., Lanz, V. A., Prevot, A. S. H. H., Baltensperger, U., Mihalopoulos, N., Laaksonen, A., Donahue, N. M. and Pandis, S. N.: Sources and atmospheric processing of organic aerosol in the Mediterranean: insights from aerosol mass spectrometer factor analysis, Atmos. Chem. Phys., 11(23), 12499–12515, doi:10.5194/acp-11-12499-2011, 2011.

Horvath, H.: Atmospheric light absorption—A review, Atmos. Environ. Part A. Gen. Top.,

27(3), 293–317, doi:10.1016/0960-1686(93)90104-7, 1993.

IPCC: Clouds and Aerosols, in Climate Change 2013 - The Physical Science Basis, edited by Intergovernmental Panel on Climate Change, pp. 571–658, Cambridge University Press, Cambridge., 2014.

Jacobson, M. C., Hansson, H.-C., Noone, K. J. and Charlson, R. J.: Organic atmospheric aerosols: Review and state of the science, Rev. Geophys., 38(2), 267–294, doi:10.1029/1998RG000045, 2000.

Jacobson, M. Z.: Global direct radiative forcing due to multicomponent anthropogenic and natural aerosols, J. Geophys. Res. Atmos., 106(D2), 1551–1568, doi:10.1029/2000JD900514, 2001.

Jimenez, J. L., Canagaratna, M. R., Donahue, N. M., Prevot, A. S. H. H., Zhang, Q., Kroll, J. H., DeCarlo, P. F., Allan, J. D., Coe, H., Ng, N. L., Aiken, A. C., Docherty, K. S., Ulbrich, I. M., Grieshop, A. P., Robinson, A. L., Duplissy, J., Smith, J. D., Wilson, K. R., Lanz, V. A., Hueglin, C., Sun, Y. L., Tian, J., Laaksonen, A., Raatikainen, T., Rautiainen, J., Vaattovaara, P., Ehn, M., Kulmala, M., Tomlinson, J. M., Collins, D. R., Cubison, M. J., Dunlea, E. J., Huffman, J. A., Onasch, T. B., Alfarra, M. R., Williams, P. I., Bower, K., Kondo, Y., Schneider, J., Drewnick, F., Borrmann, S., Weimer, S., Demerjian, K., Salcedo, D., Cottrell, L., Griffin, R., Takami, A., Miyoshi, T., Hatakeyama, S., Shimono, A., Sun, J. Y., Zhang, Y. M., Dzepina, K., Kimmel, J. R., Sueper, D., Jayne, J. T., Herndon, S. C., Trimborn, A. M., Williams, L. R., Wood, E. C., Middlebrook, A. M., Kolb, C. E., Baltensperger, U., Worsnop, D. R., Dunlea, J., Huffman, J. A., Onasch, T. B., Alfarra, M. R., Williams, P. I., Bower, K., Kondo, Y., Schneider, J., Drewnick, F., Borrmann, S., Weimer, S., Demerjian, K., Salcedo, D., Cottrell, L., Griffin, R., Takami, A., Miyoshi, T., Hatakeyama, S., Shimono, A., Sun, J. Y., Zhang, Y. M., Dzepina, K., Kimmel, J. R., Sueper, D., Jayne, J. T., Herndon, S. C., Trimborn, A. M., Williams, L. R.,

Wood, E. C., Middlebrook, A. M., Kolb, C. E., Baltensperger, U., Worsnop, D. R., Dunlea, E. J., Huffman, J. A., et al.: Evolution of organic aerosols in the atmosphere, Science (80-.)., 326(5959), 1525–1529, doi:10.1126/science.1180353, 2009.

Lanz, V. A., Alfarra, M. R., Baltensperger, U., Buchmann, B., Hueglin, C. and Prévôt, A. S. H.: Source apportionment of submicron organic aerosols at an urban site by factor analytical modelling of aerosol mass spectra, Atmos. Chem. Phys., 7(6), 1503–1522, doi:10.5194/acp-7-1503-2007, 2007.

Lanz, V. A., Alfarra, M. R., Baltensperger, U., Buchmann, B., Hueglin, C., Szidat, S., Wehrli, M. N., Wacker, L., Weimer, S., Caseiro, A., Puxbaum, H. and Prevot, A. S. H.: Source Attribution of Submicron Organic Aerosols during Wintertime Inversions by Advanced Factor Analysis of Aerosol Mass Spectra, Environ. Sci. Technol., 42(1), 214–220, doi:10.1021/es0707207, 2008.

Lelieveld, J., Evans, J. S., Fnais, M., Giannadaki, D. and Pozzer, A.: The contribution of outdoor air pollution sources to premature mortality on a global scale, Nature, 525(7569), 367–371, doi:10.1038/nature15371, 2015.

Matthew, B. M., Middlebrook, A. M. and Onasch, T. B.: Collection Efficiencies in an Aerodyne Aerosol Mass Spectrometer as a Function of Particle Phase for Laboratory Generated Aerosols, Aerosol Sci. Technol., 42(11), 884–898, doi:10.1080/02786820802356797, 2008.

Mauderly, J. L. and Chow, J. C.: Health Effects of Organic Aerosols, Inhal. Toxicol., 20(3), 257–288, doi:10.1080/08958370701866008, 2008.

Meteotest: Data Report Switzerland 2007 – 2016, Bern, Switzerland., 2017.

Minguillón, M. C., Ripoll, A., Pérez, N., Prévôt, A. S. H. H., Canonaco, F., Querol, X. and Alastuey, A.: Chemical characterization of submicron regional background aerosols in the

882 western Mediterranean using an Aerosol Chemical Speciation Monitor, Atmos. Chem. Phys.,
883 15(11), 6379–6391, doi:10.5194/acp-15-6379-2015, 2015.

884 Mohr, C., Decarlo, P. F., Heringa, M. F., Chirico, R., Slowik, J. G., Richter, R., Reche, C.,
885 Alastuey, A., Querol, X., Seco, R., Crippa, M., Zimmermann, R., Baltensperger, U., Barcelona,
886 D., Munchen, H. Z. and Mass, J.: Wintertime aerosol chemical composition and source
887 apportionment of the organic fraction in the metropolitan area of Paris, Atmos. Chem. Phys.,
888 12(4), 1649–1665, doi:10.5194/acp-13-961-2013, 2012.

889 Monn, C.: Exposure assessment of air pollutants: a review on spatial heterogeneity and
890 indoor/outdoor/personal exposure to suspended particulate matter, nitrogen dioxide and ozone,
891 Atmos. Environ., 35(1), 1–32, doi:10.1016/S1352-2310(00)00330-7, 2001.

892 Murphy, D. M., Cziczo, D. J., Froyd, K. D., Hudson, P. K., Matthew, B. M., Middlebrook, A.
893 M., Peltier, R. E., Sullivan, A., Thomson, D. S. and Weber, R. J.: Single-particle mass
894 spectrometry of tropospheric aerosol particles, J. Geophys. Res. Atmos., 111(D23), n/a-n/a,
895 doi:10.1029/2006JD007340, 2006.

896 Ng, N. L., Canagaratna, M. R., Zhang, Q., Jimenez, J. L., Tian, J., Ulbrich, I. M., Kroll, J. H.,
897 Docherty, K. S., Chhabra, P. S., Bahreini, R., Murphy, S. M., Seinfeld, J. H., Hildebrandt, L.,
898 Donahue, N. M., DeCarlo, P. F., Lanz, V. A., Prévôt, A. S. H. H., Dinar, E., Rudich, Y. and
899 Worsnop, D. R.: Organic aerosol components observed in Northern Hemispheric datasets from
900 Aerosol Mass Spectrometry, Atmos. Chem. Phys., 10(10), 4625–4641, doi:10.5194/acp-10-
901 4625-2010, 2010.

902 Ng, N. L., Herndon, S. C., Trimborn, A., Canagaratna, M. R., Croteau, P. L., Onasch, T. B.,
903 Sueper, D., Worsnop, D. R., Zhang, Q., Sun, Y. L. and Jayne, J. T.: An Aerosol Chemical
904 Speciation Monitor (ACSM) for Routine Monitoring of the Composition and Mass

905 Concentrations of Ambient Aerosol, Aerosol Sci. Technol., 45(7), 780–794,
906 doi:10.1080/02786826.2011.560211, 2011a.

907 Ng, N. L., Canagaratna, M. R., Jimenez, J. L., Zhang, Q., Ulbrich, I. M. and Worsnop, D. R.:
908 Real-Time Methods for Estimating Organic Component Mass Concentrations from Aerosol
909 Mass Spectrometer Data, Environ. Sci. Technol., 45(3), 910–916, doi:10.1021/es102951k,
910 2011b.

911 NIST Mass Spectrometry Data Center: Disulfide, dimethyl, SRD 69. [online] Available from:
912 https://webbook.nist.gov/cgi/cbook.cgi?ID=C624920&Mask=200#Refs (Accessed 6 August
913 2020), 2014.

914 Paatero, P.: The Multilinear Engine—A Table-Driven, Least Squares Program for Solving
915 Multilinear Problems, Including the n -Way Parallel Factor Analysis Model, J. Comput. Graph.
916 Stat., 8(4), 854–888, doi:10.1080/10618600.1999.10474853, 1999.

917 Paatero, P. and Hopke, P. K.: Discarding or downweighting high-noise variables in factor
918 analytic models, Anal. Chim. Acta, 490(1–2), 277–289, doi:10.1016/S0003-2670(02)01643-4,
919 2003.

920 Paatero, P., Eberly, S., Brown, S. G. and Norris, G. A.: Methods for estimating uncertainty in
921 factor analytic solutions, Atmos. Meas. Tech., 7(3), 781–797, doi:10.5194/amt-7-781-2014,
922 2014.

923 Parworth, C., Fast, J., Mei, F., Shippert, T., Sivaraman, C., Tilp, A., Watson, T. and Zhang, Q.:
924 Long-term measurements of submicrometer aerosol chemistry at the Southern Great Plains
925 (SGP) using an Aerosol Chemical Speciation Monitor (ACSM), Atmos. Environ., 106, 43–55,
926 doi:10.1016/j.atmosenv.2015.01.060, 2015.

927 Petit, J.-E. E., Favez, O., Sciare, J., Canonaco, F., Croteau, P., Močnik, G., Jayne, J., Worsnop,

928 D. and Leoz-Garziandia, E.: Submicron aerosol source apportionment of wintertime pollution
929 in Paris, France by double positive matrix factorization (PMF2) using an aerosol chemical
930 speciation monitor (ACSM) and a multi-wavelength Aethalometer, Atmos. Chem. Phys.,
931 14(24), 13773–13787, doi:10.5194/acp-14-13773-2014, 2014.

932 Pfaffenberger, L., Barmet, P., Slowik, J. G., Praplan, A. P., Dommen, J., Prévôt, A. S. H. and
933 Baltensperger, U.: The link between organic aerosol mass loading and degree of oxygenation:
934 an α-pinene photooxidation study, Atmos. Chem. Phys., 13(13), 6493–6506, doi:10.5194/acp-
935 13-6493-2013, 2013.

936 Pope, C. A. and Dockery, D. W.: Health Effects of Fine Particulate Air Pollution: Lines that
937 Connect, J. Air Waste Manage. Assoc., 56(6), 709–742,
938 doi:10.1080/10473289.2006.10464485, 2006.

939 Ramanathan, V., Chung, C., Kim, D., Bettge, T., Buja, L., Kiehl, J. T., Washington, W. M., Fu,
940 Q., Sikka, D. R. and Wild, M.: Atmospheric brown clouds: Impacts on South Asian climate
941 and hydrological cycle, Proc. Natl. Acad. Sci., 102(15), 5326–5333,
942 doi:10.1073/pnas.0500656102, 2005.

943 Reyes-Villegas, E., Green, D. C., Priestman, M., Canonaco, F., Coe, H., Prévôt, A. S. H. H.
944 and Allan, J. D.: Organic aerosol source apportionment in London 2013 with ME-2: Exploring
945 the solution space with annual and seasonal analysis, Atmos. Chem. Phys., 16(24), 15545–
946 15559, doi:10.5194/acp-16-15545-2016, 2016.

947 Ripoll, A., Minguillón, M. C., Pey, J., Jimenez, J. L., Day, D. A., Sosedova, Y., Canonaco, F.,
948 Prévôt, A. S. H., Querol, X. and Alastuey, A.: Long-term real-time chemical characterization
949 of submicron aerosols at Montsec (southern Pyrenees, 1570 m a.s.l.), Atmos. Chem. Phys.,
950 15(6), 2935–2951, doi:10.5194/acp-15-2935-2015, 2015.

951 von Schneidemesser, E., Monks, P. S., Allan, J. D., Bruhwiler, L., Forster, P., Fowler, D., Lauer,
952 A., Morgan, W. T., Paasonen, P., Righi, M., Sindelarova, K. and Sutton, M. A.: Chemistry and
953 the Linkages between Air Quality and Climate Change, Chem. Rev., 115(10), 3856–3897,
954 doi:10.1021/acs.chemrev.5b00089, 2015.

955 Schurman, M. I., Lee, T., Sun, Y., Schichtel, B. A., Kreidenweis, S. M. and Collett Jr., J. L.:
956 Investigating types and sources of organic aerosol in Rocky Mountain National Park using
957 aerosol mass spectrometry, Atmos. Chem. Phys., 15(2), 737–752, doi:10.5194/acp-15-737-
958 2015, 2015.

959 Schwarz, J. P., Gao, R. S., Perring, A. E., Spackman, J. R. and Fahey, D. W.: Black carbon
960 aerosol size in snow, Sci. Rep., 3, 1–5, doi:10.1038/srep01356, 2013.

961 Sug Park, E., Henry, R. C. and Spiegelman, C. H.: Estimating the number of factors to include
962 in a high-dimensional multivariate bilinear model, Commun. Stat. - Simul. Comput., 29(3),
963 723–746, doi:10.1080/03610910008813637, 2000.

964 Szidat, S., Prévôt, A. S. H., Sandradewi, J., Alfarra, M. R., Synal, H.-A., Wacker, L. and
965 Baltensperger, U.: Dominant impact of residential wood burning on particulate matter in
966 Alpine valleys during winter, Geophys. Res. Lett., 34(5), doi:10.1029/2006GL028325, 2007.

967 The Swiss Federal Council: Ordinance of 16 December 1985 on Air Pollution Control (OAPC).
968 [online] Available from: https://www.admin.ch/opc/en/classified-
969 compilation/19850321/index.html#app7 (Accessed 10 September 2019), 2018.

970 Tobler, A., Bhattu, D., Canonaco, F., Lalchandani, V., Shukla, A., Thamban, N. M., Mishra,
971 S., Srivastava, A. K., Bisht, D. S., Tiwari, S., Singh, S., Močnik, G., Baltensperger, U., Tripathi,
972 S. N., Slowik, J. G. and Prévôt, A. S. H.: Chemical characterization of PM2.5 and source
973 apportionment of organic aerosol in New Delhi, India, Sci. Total Environ., 745, 140924,

974 doi:10.1016/j.scitotenv.2020.140924, 2020.

975 Ulbrich, I. M., Canagaratna, M. R., Zhang, Q., Worsnop, D. R. and Jimenez, J. L.:
976 Interpretation of organic components from Positive Matrix Factorization of aerosol mass
977 spectrometric data, Atmos. Chem. Phys., 9(9), 2891–2918, doi:10.5194/acp-9-2891-2009,
978 2009.

979 Allan, J. D., Delia, A. E., Coe, H., Bower, K. N., Alfarra, M. R. R., Jimenez, J. L., Middlebrook,
980 A. M., Drewnick, F., Onasch, T. B., Canagaratna, M. R., Jayne, J. T. and Worsnop, D. R.: A
981 generalised method for the extraction of chemically resolved mass spectra from Aerodyne
982 aerosol mass spectrometer data, J. Aerosol Sci., 35(7), 909–922,
983 doi:10.1016/j.jaerosci.2004.02.007, 2004.

984 Canonaco, F., Slowik, J. G., Baltensperger, U. and Prévôt, A. S. H.: Seasonal differences in
985 oxygenated organic aerosol composition: implications for emissions sources and factor
986 analysis, Atmos. Chem. Phys., 15(12), 6993–7002, doi:10.5194/acp-15-6993-2015, 2015.

987 Canonaco, F., Tobler, A., Chen, G., Sosedova, Y., Slowik, J. G. G., Bozzetti, C., Daellenbach,
988 K. R., El Haddad, I., Crippa, M., Huang, R.-J., Furger, M., Baltensperger, U., Prévôt, A. S. H.,
989 Kaspar Rudolf Haddad, I. E. D., Crippa, M., Huang, R.-J., Furger, M., Baltensperger, U.,
990 Prevot, A. S. H., Daellenbach, Kaspar Rudolf Haddad, I. El, Crippa, M., Huang, R.-J., Furger,
991 M., Baltensperger, U. and Prevot, A. S. H.: A new method for long-term source apportionment
992 with time-dependent factor profiles and uncertainty assessment using SoFi Pro: application to
993 1 year of organic aerosol data, Atmos. Meas. Tech., 14(2), 923–943, doi:10.5194/amt-14-923-
994 2021, 2021.

995 Crippa, M., Canonaco, F., Lanz, V. A., Äijälä, M., Allan, J. D., Carbone, S., Capes, G.,
996 Ceburnis, D., Dall'Osto, M., Day, D. A., DeCarlo, P. F., Ehn, M., Eriksson, A.,

997 Freney, E., Hildebrandt Ruiz, L., Hillamo, R., Jimenez, J. L., Junninen, H., Kiendler-Scharr,
998 A., Kortelainen, A.-M. M., Kulmala, M., Laaksonen, A., Mensah, A. A., Mohr, C., Nemitz, E.,
999 O'Dowd, C., Ovadnevaite, J., Pandis, S. N., Petäjä, T., Poulain, L., Saarikoski, S.,
1000 Sellegri, K., Swietlicki, E., Tiitta, P., Worsnop, D. R., Baltensperger, U., Prévôt, A. S. H. H.,
1001 Dall'Osto, M., Day, D. A., DeCarlo, P. F., Ehn, M., Eriksson, A., Freney, E., Hildebrandt Ruiz,
1002 L., Hillamo, R., Jimenez, J. L., Junninen, H., Kiendler-Scharr, A., Kortelainen, A.-M. M.,
1003 Kulmala, M., Laaksonen, A., Mensah, A. A., Mohr, C., Nemitz, E., O'Dowd, C., Ovadnevaite,
1004 J., Pandis, S. N., Petäjä, T., Poulain, L., Saarikoski, S., Sellegri, K., Swietlicki, E., Tiitta, P.,
1005 Worsnop, D. R., Baltensperger, U. and Prévôt, A. S. H. H.: Organic aerosol components
1006 derived from 25 AMS data sets across Europe using a consistent ME-2 based source
1007 apportionment approach, Atmos. Chem. Phys., 14(12), 6159–6176, doi:10.5194/acp-14-6159-
1008 2014, 2014.

1009 Daellenbach, K. R., Bozzetti, C., Křepelová, A., Canonaco, F., Wolf, R., Zotter, P., Fermo, P.,
1010 Crippa, M., Slowik, J. G., Sosedova, Y., Zhang, Y., Huang, R.-J. J., Poulain, L., Szidat, S.,
1011 Baltensperger, U., El Haddad, I. and Prévôt, A. S. H. H.: Characterization and source
1012 apportionment of organic aerosol using offline aerosol mass spectrometry, Atmos. Meas. Tech.,
1013 9(1), 23–39, doi:10.5194/amt-9-23-2016, 2016.

1014 Dämmgen, U., Thöni, L., Lumpp, R., Gilke, K., Seitler, E. and Bullinger, M.: Feldexperiment
1015 zum Methoden- vergleich von Ammoniak- und messungen in der Umgebungsluft , 2005 bis
1016 2008 in Braunschweig, vTI Agric. For. Res. - Sonderh., (337), 62 [online] Available from:
1017 https://www.thuenen.de/media/publikationen/landbauforschung-sonderhefte/lbf_sh337.pdf,
1018 2010.

1019 Docherty, K. S., Lewandowski, M. and Jimenez, J. L.: Effect of Vaporizer Temperature on
1020 Ambient Non-Refractory Submicron Aerosol Composition and Mass Spectra Measured by the

Aerosol Mass Spectrometer, Aerosol Sci. Technol., 49(7), 485–494, doi:10.1080/02786826.2015.1042100, 2015.

Hildebrandt, L., Kostenidou, E., Lanz, V. A., Prevot, A. S. H. H., Baltensperger, U., Mihalopoulos, N., Laaksonen, A., Donahue, N. M. and Pandis, S. N.: Sources and atmospheric processing of organic aerosol in the Mediterranean: insights from aerosol mass spectrometer factor analysis, Atmos. Chem. Phys., 11(23), 12499–12515, doi:10.5194/acp-11-12499-2011, 2011.

Ng, N. L., Canagaratna, M. R., Zhang, Q., Jimenez, J. L., Tian, J., Ulbrich, I. M., Kroll, J. H., Docherty, K. S., Chhabra, P. S., Bahreini, R., Murphy, S. M., Seinfeld, J. H., Hildebrandt, L., Donahue, N. M., DeCarlo, P. F., Lanz, V. A., Prévôt, A. S. H. H., Dinar, E., Rudich, Y. and Worsnop, D. R.: Organic aerosol components observed in Northern Hemispheric datasets from Aerosol Mass Spectrometry, Atmos. Chem. Phys., 10(10), 4625–4641, doi:10.5194/acp-10-4625-2010, 2010.

NIST Mass Spectrometry Data Center: Disulfide, dimethyl, SRD 69. [online] Available from: https://webbook.nist.gov/cgi/cbook.cgi?ID=C624920&Mask=200#Refs (Accessed 6 August 2020), 2014.

Via, M. et al.: Comparison between rolling and seasonal PMF techniques for organic aerosol source apportionment [Unpublished manuscript]., 2021.

Vlachou, A., Daellenbach, K. R., Bozzetti, C., Chazeau, B., Salazar, G. A., Szidat, S., Jaffrezo, J.-L., Hueglin, C., Baltensperger, U., Haddad, I. El and Prévôt, A. S. H.: Advanced source apportionment of carbonaceous aerosols by coupling offline AMS and radiocarbon size-segregated measurements over a nearly 2-year period, Atmos. Chem. Phys., 18(9), 6187–6206, doi:10.5194/acp-18-6187-2018, 2018.

Zhang, Q., Jimenez, J. L., Canagaratna, M. R., Allan, J. D., Coe, H., Ulbrich, I., Alfarra, M. R., Takami, A., Middlebrook, A. M., Sun, Y. L., Dzepina, K., Dunlea, E., Docherty, K., DeCarlo, P. F., Salcedo, D., Onasch, T., Jayne, J. T., Miyoshi, T., Shimono, A., Hatakeyama, S., Takegawa, N., Kondo, Y., Schneider, J., Drewnick, F., Borrmann, S., Weimer, S., Demerjian, K., Williams, P., Bower, K., Bahreini, R., Cottrell, L., Griffin, R. J., Rautiainen, J., Sun, J. Y., Zhang, Y. M. and Worsnop, D. R.: Ubiquity and dominance of oxygenated species in organic aerosols in anthropogenically-influenced Northern Hemisphere midlatitudes, Geophys. Res. Lett., 34(13), n/a-n/a, doi:10.1029/2007GL029979, 2007.

Zhang, Q., Jimenez, J. L., Canagaratna, M. R., Ulbrich, I. M., Ng, N. L., Worsnop, D. R. and Sun, Y.: Understanding atmospheric organic aerosols via factor analysis of aerosol mass spectrometry: a review, Anal. Bioanal. Chem., 401(10), 3045–3067, doi:10.1007/s00216-011-5355-y, 2011.

Zhang, Y., Favez, O., Petit, J.-E., Canonaco, F., Truong, F., Bonnaire, N., Crenn, V., Amodeo, T., Prévôt, A. S. H., Sciare, J., Gros, V. and Albinet, A.: Six-year source apportionment of submicron organic aerosols from near-continuous highly time-resolved measurements at SIRTA (Paris area, France), Atmos. Chem. Phys., 19(23), 14755–14776, doi:10.5194/acp-19-14755-2019, 2019.

Zotter, P., Herich, H., Gysel, M., El-Haddad, I., Zhang, Y., Močnik, G., Hüglin, C., Baltensperger, U., Szidat, S., Prévôt, A. S. H. H., Mocnik, G., Hüglin, C., Baltensperger, U., Szidat, S., Prévôt, A. S. H. H., Močnik, G., Hüglin, C., Baltensperger, U., Szidat, S. and Prévôt, A. S. H. H.: Evaluation of the absorption Ångström exponents for traffic and wood burning in the Aethalometer-based source apportionment using radiocarbon measurements of ambient aerosol, Atmos. Chem. Phys., 17(6), 4229–4249, doi:10.5194/acp-17-4229-2017, 2017.